

Studies of nonadiabatic dynamics in the singlet fission processes of pentacene dimer via tensor network method

Cite as: J. Chem. Phys. 159, 224301 (2023); doi: 10.1063/5.0174416

Submitted: 30 August 2023 • Accepted: 12 November 2023 •

Published Online: 8 December 2023



Jiawei Peng,^{1,2,3} Deping Hu,⁴ Hong Liu,^{2,3,a)} Qiang Shi,⁵ Peng Bao,⁵ and Zhenggang Lan^{2,3,b)}

AFFILIATIONS

¹ School of Chemistry, South China Normal University, Guangzhou 510006, China

² MOE Key Laboratory of Environmental Theoretical Chemistry, South China Normal University, Guangzhou 510006, China

³ SCNU Environmental Research Institute, Guangdong Provincial Key Laboratory of Chemical Pollution and Environmental Safety, School of Environment, South China Normal University, Guangzhou 510006, China

⁴ Center for Advanced Materials Research, Beijing Normal University, Zhuhai 519087, China

⁵ Beijing National Laboratory for Molecular Sciences, State Key Laboratory for Structural Chemistry of Unstable and Stable Species, Institute of Chemistry, Chinese Academy of Sciences, No. 2 North 1st Street, Zhongguancun, Beijing 100190, China

^{a)}E-mail: hongliu@m.scnu.edu.cn

^{b)}Author to whom correspondence should be addressed: zhenggang.lan@m.scnu.edu.cn and zhenggang.lan@gmail.com

ABSTRACT

Singlet fission (SF) is a very significant photophysical phenomenon and possesses potential applications. In this work, we try to give a rather detailed theoretical investigation of the SF process in the stacked polyacene dimer by combining the high-level quantum chemistry calculations and the quantum dynamics simulations based on the tensor network method. Starting with the construction of the linear vibronic coupling model, we explore the pure electronic dynamics and the vibronic dynamics in the SF processes. The role of vibrational modes in nonadiabatic dynamics is addressed. The results show that the super-exchange mechanism mediated by the charge-transfer state is found in both pure electronic dynamics and the nonadiabatic dynamics. Particularly the vibrational modes with the frequencies resonance with the adiabatic energy gap play very import roles in the SF dynamics. This work not only provides a deep and detailed understanding of the SF process but also verifies the efficiency of the tensor network method with the train structure that can serve as the reference dynamics method to explore the dynamics behaviors of complex systems.

Published under an exclusive license by AIP Publishing. <https://doi.org/10.1063/5.0174416>

I. INTRODUCTION

Singlet fission (SF) is a very significant photophysical phenomenon in a group of organic photovoltaic materials, such as covalent dimers (tetracene,¹ pentacene,² diphenylisobenzofuran,³ etc.^{4–6}), polyenes and carotenoids,⁷ conjugated polymers,⁸ and molecular solids (thin film or crystal),⁸ due to its huge potential to boost the quantum yield of solar energy conversation.^{9–13} In the SF process, one singlet exciton is split into a pair of coupled triplet excitons and then converted into two noninteracting triplet states. The SF process is spin-allowed since the two produced triplets are coupled into an overall singlet state. This indicates that the SF

reaction may take place in the ultrafast time domain from the femtosecond to the picosecond timescale, which is usually not affected by the nanosecond-scale radiative decay.^{9–13} In principle, if some organic photovoltaic materials with efficient SF reactions are properly designed, it is possible to go beyond the Shockley–Queisser limit,¹⁴ largely improve the photoelectric conversion efficiency, and promote the commercial application of organic photovoltaic devices.^{9,15} To achieve this goal, the exploration of the intrinsic nature behind the SF process becomes essential.

In the past decade, extensive experimental and theoretical effects have been devoted to this research area.^{4,16–101} Experimentally, time-resolved spectra techniques, like ultrafast pump-

probe,^{19,38,65,71} two-dimensional electronic spectroscopies,^{66,72} and two-photon photoemission spectroscopies,^{29,34,71} were gradually employed to study the SF reaction of different systems, including thin films or crystals of tetracene, pentacene, and diphenylisobenzofuran, etc. The relevant measurements and analyses largely identify that the multiexciton state plays a potential role in the SF process. In addition, the SF dynamics in different systems may take place on various time scales, from the femtosecond to the picosecond domains.^{9–13}

Theoretically, with the development of high-level quantum chemistry theory, precise electronic structure calculations can be performed in the SF materials, and the effective model Hamiltonian can be constructed and analyzed.^{74,80,83–94,102–104} For instance, the relative energetics of the low-lying states of the pentacene monomer were once investigated by various electronic structure methods.^{9–13,74} Particularly, the pentacene dimer receives considerable research attention because it provides a prototype to study the SF mechanism. Different strategies were proposed to construct the diabatic Hamiltonian of pentacene dimers. For instance, the diabatic Hamiltonian matrix elements were formulated by Smith and Michl based on a minimum configuration space;⁹ the electronic diabatic couplings were approximated by Berkelbach et al. in terms of the Fock matrix elements of the HOMO and LUMO of two pentacene molecules;⁸⁴ the possible nonadiabatic coupling between the single and multiexciton states for pentacene dimers was constructed by Feng *et al.*,¹⁰⁵ a five-state model Hamiltonian was constructed by Liang and co-workers in terms of the time-dependent density function theory to investigate the J- and H-aggregate behavior;⁹³ an *ab initio* exciton model was presented by Martínez and co-workers, in which the Frenkel exciton model was further extended, including valence, charge-transfer, and multiexcitonic excited states.⁹⁴ The SF model Hamiltonian was also built from the multistate density functional theory developed by Gao and co-workers.⁸⁰

Besides, different dynamics methods, from the exact full-quantum to semi-classical ones, were used to simulate the SF reaction and explore the possibility of various mechanisms proposed.^{73,74,79,83,85,86,88,92,93,103,106–114} For example, several groups, including Ratner,^{103,108} Teichen and Eaves,⁸³ Reichman,^{85,86,88,107} and Grozema,^{115,116} used the quantum master equation method based on the reduced density matrix to explore the intrinsic mechanism behind the SF reaction. Zhao and co-workers once employed the stochastic Schrödinger equation to study the SF dynamics.⁹³ The ultrafast nonadiabatic dynamics for the SF process were also extensively investigated by using the quantum dynamics methods that treat all involved electronic and nuclear degrees of freedom explicitly.^{60,73,74,79,114} Different quantum dynamics approaches were taken, such as the multilayer multiconfigurational time-dependent Hartree method by Burghardt, Tamura and co-workers,⁶⁰ Thoss and co-workers,⁷³ and ourselves.¹¹⁴ Recently, the tensor network method was also employed by several groups^{74,79,95} to study the ultrafast SF process. For example, the pioneer work by Chin and co-workers provides many important insights into SF dynamics, in which a full five-level diabatic model for the pentacene derivative was used to explore the SF reaction based on the machine-learning technique and tensor network method with the tree structure. This is the first work to use the tensor network method to study the full quantum dynamics of the five-state SF model. The trajectory-based method is also a practical way to treat the SF dynamics in complex systems.

For instance, Tao used the symmetrical quasi-classical dynamics method to study the influence of different conditions on the SF dynamics;^{92,109,110} Akimov and co-workers used the trajectory surface hopping method to investigate the nonadiabatic dynamics of charge transfer and SF at the pentacene/C₆₀ interface.¹¹¹

With the help of these important pioneer explorations, a basic knowledge framework about the SF process is constructed.^{9–13} There is no doubt that the intermediate multi-exciton state plays an extremely important role in the SF reaction; therefore, its basic properties, dissociation, and formation processes are usually the focus of many studies. The previous works reveal that the involvement of the multi-exciton state is essential to the SF dynamics, which is an entangled triplet-state pair TT, i.e., two triplets coupling with each other to form an overall spin singlet.

The formation mechanism of the TT state has long been the focus of scientific debate.^{9–13} To date, it is widely accepted that the TT formation is highly system-specific, and two mechanisms are commonly used for understanding the intrinsic characteristics involved in the SF reaction, especially for the short-time dynamics. One is the direct mechanism via a two-electron process, in which the local excited state LE is directly decayed into the TT state. The other is the mediated mechanism in terms of two one-electron processes, in which the intermediate charge transfer state CT acts as a bridge for the transformation from the LE state to the TT state and plays a significant regulatory role in the SF reaction.

Although the existing experimental and theoretical advances provide much evidence for inferring or different perspectives for understanding the inherent mechanism behind the SF process, it is still not enough to uncover overall microscopic physical insights into the SF reaction. As research continues, it is important to study the rather complex many-body problem involving the interplay between vibrational and electronic degrees of freedom in the SF dynamics. This target requires two efforts. First, it is necessary to build reasonable models that include all relevant electronic states (the LE, CT, and TT states) and important nuclear degrees of freedom. Preferably, all parameters in the model should be very accurate to describe realistic systems, which should be derived from the high-level electronic structure calculations. Second, an accurate quantum dynamics study should be performed to treat all nuclear and electronic degrees of freedom with equal root. By doing so, it is possible to provide a very detailed understanding of coupled electronic-nuclear motions in the SF dynamics of realistic systems.

In this paper, we try to provide a rather accurate description of the SF process in the pentacene dimer by using electronic-structure and quantum dynamics calculations. First, a linear vibronic coupling model Hamiltonian was constructed, which includes five electronic states (two LE states, two CT states, and one TT state) and all intramolecular vibrational degrees of freedom of the system. Since diabatization is not an easy task for the current system, we employ the five-state electronic Hamiltonian built from the state averaged extended multi-configurational quasi-degenerate perturbation theory (XMCQDPT) by Zeng *et al.*⁸⁹ Next, the additional high-level extended multi-state complete active space second order perturbation theory (XMS-CASPT2)¹¹⁷ was employed to get the vibronic coupling parameters in the diabatic Hamiltonian. Finally, the full quantum dynamics of the SF dynamics was simulated by using the recently developed tensor network method with the train structure. In the tensor train format,^{118,119} the quantum state and operator

are expressed as different matrix products, respectively. Since the high-order tensors are decomposed into a series of localized low-order and low-rank ones, the curse of dimensionality can be greatly alleviated, and the computational costs can also be largely reduced. Therefore, the tensor network approach with the train structure should be a very efficient and powerful algorithm to simulate the full quantum evolution of complex many-body systems with many coupled degrees of freedom. In this sense, it is possible to employ such an approach to study the SF dynamics of pentacene dimers. Particularly, this approach allows us to provide a very detailed analysis of roles of the quantum coherence, vibronic couplings, and dissipation effects in the SF dynamics. Overall, this work provides a deep and detailed understanding of the SF dynamics in pentacene dimers and relevant systems.

II. THEORETICAL METHODS AND COMPUTATIONAL DETAILS

A. Model Hamiltonian

1. Diabatic Hamiltonian

In order to effectively discuss the SF dynamics of the pentacene dimer here, the molecular Hamiltonian employed in the present work includes five low-lying singlet excited electronic states, namely, two *LE* states (S_0S_1 and S_1S_0), two *CT* states (CA and AC), and one triplet-triplet coupled singlet state TT. The nuclear motion was described by a set of dimensionless normal modes, and all intramolecular vibrational degrees of freedom were retained. The linear vibronic-coupling Hamiltonian was considered to construct the diabatic model.¹²⁰ In the current case, the total Hamiltonian \hat{H}_d is written as the summation of the kinetic and diabatic potential operators, namely,

$$\begin{aligned} \hat{H}_d &= \hat{T} + \hat{V}_d, \\ \hat{T} &= \sum_i^{N_b} \frac{1}{2} \omega_i \hat{P}_i^2, \\ \hat{V}_d &= \sum_k \sum_l |\psi_k\rangle V_{kl} \langle \psi_l|, \\ V_{kk} &= V_k^{(0)} + \sum_i^{N_b} \frac{1}{2} \omega_i Q_i^2 + \sum_i \kappa_i^{(k)} Q_i, \end{aligned} \quad (1)$$

where $\psi_k(\psi_l)$ denotes the electronic state involved. V_{kk} represents the corresponding energy of ψ_k . $V_{kl}(k \neq l)$ is the interstate diabatic coupling between ψ_k and ψ_l . \hat{P}_i and Q_i are the corresponding momentum operator and position of the vibrational mode with frequency ω_i , respectively, under the dimensionless normal coordinates. $V_k^{(0)}$ is the vertical energy of the diabatic state. $\kappa_i^{(k)}$ characterizes the vibronic coupling between the k th electronic state and the i th mode. N_b represents the number of vibrational modes.

2. Diabatic electronic states and their couplings

The parameters in the diabatic Hamiltonian, including the energies of different electronic states ($V_k^{(0)}$) at $Q_i = 0$ and the diabatic couplings (V_{kl}), were directly taken from the previous work by Zeng *et al.*,⁸⁹ and their values can be found in Table I of the Appendix. The reason is that the electronic Hamiltonian in their

TABLE I. The parameters V_{kl} in the molecular Hamiltonian (in eV). Here, the energy of the S_0S_0 state is set to 0.000 eV, and the number in the bracket denotes the index of the state order in the calculations.

	S_0S_0 (0)	S_1S_0 (1)	S_0S_1 (2)	AC (3)	CA (4)	TT (5)
S_0S_0 (0)	0.000	0.000	0.000	0.000	0.000	0.000
S_1S_0 (1)	0.000	2.005	-0.006	0.099	0.079	0.000
S_0S_1 (2)	0.000	-0.006	2.010	0.075	0.086	0.001
AC (3)	0.000	0.099	0.075	2.266	0.001	-0.090
CA (4)	0.000	0.079	0.086	0.001	3.063	0.064
TT (5)	0.000	0.000	0.001	-0.090	0.064	1.900

work was obtained by the XMCQDPT method with high accuracy, which gives an excellent explanation of experimental results and agrees well with other theoretical simulations. It is worth noting that the energy difference between CA and AC states is rather large, which is due to the asymmetric geometrical alignment of the two monomers. A similar phenomenon was also noted in previous works based on different electronic structure methods.^{84,94} This indicates that CT states may play different roles in the SF dynamics. The ground state S_0S_0 is well separated from other electronic states; therefore, this state is not included.

Again, we wish to emphasize that the construction of the diabatic model in the current system is not a trivial task, particularly as the model involves five electronic states and the TT state shows the double excitation characters. As the model by Zeng *et al.* gives a good description of the SF dynamics of the current system, we decide to simply take it. The possible influence of the parameters in the model Hamiltonian on the SF dynamics will be discussed in Sec. II A 3.

3. Vibronic couplings

In the current system, the SF process of pentacene takes place within a very short time scale after initial photoexcitation. As discussed in previous works,^{93,114} the motion of the intermolecular vibrational mode is usually relatively slow, which can be separated from the current ultrafast SF dynamics. Therefore, to simplify the model, we only consider the intramolecular vibrational modes in the construction of the diabatic Hamiltonian. The vibrational modes of each monomer were used as the basis to characterize vibronic couplings. From the monomer, the normal mode analysis at the ground state minimum was performed, and all modes were included. On this basis, all parameters for the vibronic couplings were obtained with the assistance of our own high-level electronic structure calculations.

The vibronic coupling constants $\{\kappa_i^{(k)}\}$ are obtained by the transformation of the gradient from Cartesian coordinates to dimensionless normal ones,¹²⁰ i.e.,

$$\boldsymbol{\kappa} = -\mathbf{f}\mathbf{L}, \quad (2)$$

where \mathbf{f} is the corresponding force matrix acting on each atom in Cartesian coordinates on the relevant excited state at the equilibrium geometry of the monomer, and \mathbf{L} is the transformation matrix between Cartesian and dimensionless normal coordinates. Different approaches were used to obtain the vibronic coupling terms for different states.

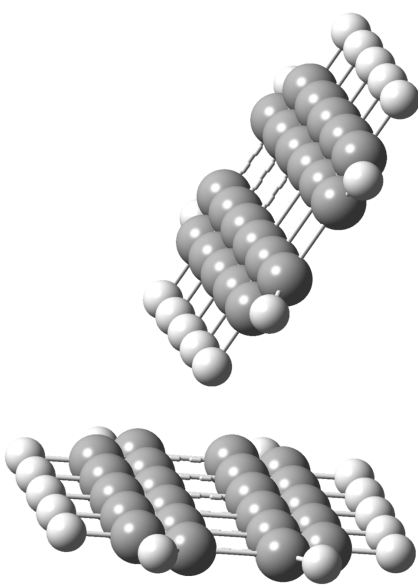


FIG. 1. The structure of pentacene dimer.

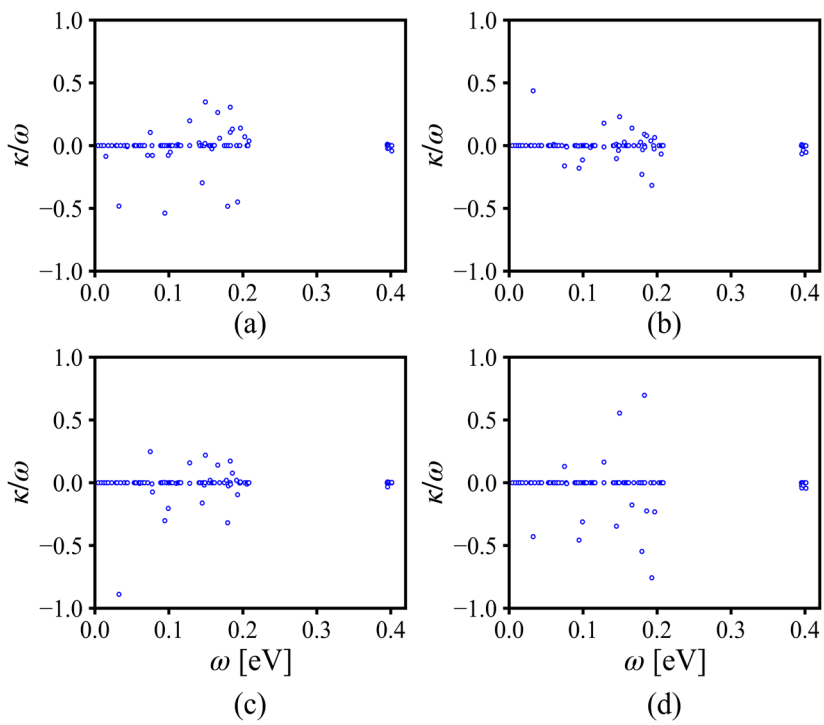
For the *LE* state, only one molecule in the pentacene dimer is excited, thus the gradient of the monomer in the excited state just needs to be calculated. For the modes that belong to the same monomer with the excitation, the $\kappa_i^{(k)}$ values are constructed by the

formula earlier. For the modes that belong to the other monomer lying in the ground state, their $\kappa_i^{(k)}$ values are naively set to zero.

For the *CT* states, both *CA* and *AC* can be viewed as a combination of the positive ion (*C*) and the negative one (*A*). With this assumption, the gradients of positive and negative ions are calculated to get $\kappa_i^{(k)}$ for the corresponding ion fragment, respectively. Then, we simply combine them together to give all the vibronic coupling terms of the *CT* states.

For the *TT* state, it can also be treated as two triplet states on the respective monomer, and the same strategy can be used to approximate the vibronic coupling.

There is no doubt that the above-mentioned method is certainly an imperfect one for generating all vibronic coupling terms since the intermolecular interaction between monomers is missing. The current construction strategy is adopted for two reasons. On the one hand, all intermolecular vibrational modes with very low frequencies should show rather large anharmonicity, while the current approach is not accurate enough to obtain a precise description of these modes. On the other hand, the SF dynamics of the pentacene dimer take place very quickly, while the low-frequency intermolecular vibrational modes should not be in resonance with the electronic dynamics due to different time scales. As a consequence, these low-frequency modes should not play a direct role here. Overall, the current model should already capture all necessary features to treat the ultrafast SF dynamics of the pentacene dimer. Certainly, in more completed treatments, the influence of these modes can be further included by introducing the static disorder.

FIG. 2. The κ/ω values of different dimensionless normal modes for the pentacene monomer: (a) singlet excited state, (b) cationic state, (c) anionic state, and (d) triplet state.

B. Quantum dynamics

1. Tensor network method

The tensor network is a very efficient full quantum dynamics method that has some variations according to the differences in network structure.^{74,119,121} In the tensor network method with the train framework,^{119,122–124} the matrix-product state (MPS) can be used to reconstruct the quantum state,

$$|\Psi\rangle = \sum_{\{s_i\}} A^{s_1} \cdots A^{s_i} \cdots A^{s_m} |s_1 \cdots s_i \cdots s_m\rangle, \quad (3)$$

where the set $\{|s_i\rangle\}$ includes m local bases, and the site-dependent tensor A^{s_i} has the $\alpha_{i-1} \times s_i \times \alpha_i$ ($\alpha_0 = \alpha_m = 1$) dimension. Due to the invariance of gauge transformation, the MPS possesses diverse representations, including the left, right, and mixed canonical forms,

$$\begin{aligned} |\Psi\rangle &= \sum_{\{s_i\}} L^{s_1} \cdots L^{s_i} \cdots L^{s_m} |s_1 \cdots s_i \cdots s_m\rangle, \\ &= \sum_{\{s_i\}} R^{s_1} \cdots R^{s_i} \cdots R^{s_m} |s_1 \cdots s_i \cdots s_m\rangle, \\ &= \sum_{\alpha_{i-1}, s_i, \alpha_i} [M^{s_i}]_{\alpha_{i-1}, \alpha_i} |\Psi_{L, \alpha_{i-1}}^{[1:i-1]}\rangle |s_i\rangle |\Psi_{R, \alpha_i}^{[i+1:m]}\rangle, \end{aligned} \quad (4)$$

where L^{s_i} and R^{s_i} represent the left and right orthonormal tensors, respectively, M^{s_i} is the i th-site center block, and $|\Psi_{L, \alpha_{i-1}}^{[1:i-1]}\rangle$ and $|\Psi_{R, \alpha_i}^{[i+1:m]}\rangle$ correspond to the intermediate states generated in the left and right orthonormal representations, respectively.

Following an analogous strategy, the matrix product operator (MPO) can also be reformulated,

$$\begin{aligned} \hat{O} &= \sum_{\{s_i\}, \{\beta'_i\}, \{\beta_i\}} W^{s_1, s'_1} \cdots W^{s_i, s'_i} \cdots W^{s_m, s'_m} |s_1 \cdots s_i \cdots s_m\rangle \\ &\times \langle s'_1 \cdots s'_i \cdots s'_m|, \end{aligned} \quad (5)$$

where the site-dependent tensor W^{s_i, s'_i} has the $\beta_{i-1} \times s_i \times s'_i \times \beta_i$ ($\beta_0 = \beta_m = 1$) dimension. Since the local basis can be chosen in different formats, the MPO itself is not always unique, which leads to some different construction strategies developed in recent years.¹²⁵ In the current work, the electron–phonon Hamiltonian was first reformulated in terms of the second quantization, and then the occupation number representation was used to construct the MPO.

By means of the above matrix product representations, several algorithms were proposed to propagate the time-dependent Schrödinger equation (TDSE).¹¹⁹ In the current work, the time-dependent variational principle (TDVP) method was employed to simulate the dynamics process due to its very high efficiency and accuracy.¹¹⁹ Overall, the TDVP algorithm realizes that the evolution of the quantum state is conducted in a confined MPS manifold, and the specific mathematical details can be referred to the important articles and reviews.¹¹⁹ While in implementation, the original TDSE was transformed and solved by following two equations:

$$\begin{aligned} i\hbar \frac{d}{dt} |\Psi(t)\rangle &= \sum_{i=1}^m \hat{P}_{i-1}^L \otimes \hat{I}_i \otimes \hat{P}_{i+1}^R \hat{H} |\Psi(t)\rangle, \\ i\hbar \frac{d}{dt} |\Psi(t)\rangle &= - \sum_{i=1}^{m-1} \hat{P}_i^L \otimes \hat{P}_{i+1}^R \hat{H} |\Psi(t)\rangle, \end{aligned} \quad (6)$$

where \hat{P}_i^L and \hat{P}_i^R are the left and right projectors, respectively, and satisfy

$$\begin{aligned} \hat{P}_i^L &= \sum_{\alpha_i} |\Psi_{L, \alpha_i}^{[1:i]}\rangle \langle \Psi_{L, \alpha_i}^{[1:i]}|, \\ \hat{P}_i^R &= \sum_{\alpha_i} |\Psi_{R, \alpha_{i-1}}^{[i:m]}\rangle \langle \Psi_{R, \alpha_{i-1}}^{[i:m]}|. \end{aligned} \quad (7)$$

Therefore, one needs to individually and sequentially calculate the m forward-propagation and $m - 1$ backward-propagation equations in a single step propagation.

2. Initial conditions

In the time-dependent dynamics propagation, the system was assumed to be prepared by vertical placing the lowest vibrational level of the ground state to one of the local excited states or their superposition, i.e.,

$$|\Psi(t=0)\rangle = [c_{S_0 S_1} |\Psi_{S_0 S_1}\rangle + c_{S_1 S_0} |\Psi_{S_1 S_0}\rangle] |\mathbf{0}\rangle, \quad (8)$$

where $c_{S_0 S_1}$ and $c_{S_1 S_0}$ are the coefficients corresponding to the electronic wave functions $|\Psi_{S_0 S_1}\rangle$ and $|\Psi_{S_1 S_0}\rangle$, respectively. The lowest vibrational state $|\mathbf{0}\rangle$ on the ground electronic state is given as

$$|\mathbf{0}\rangle = |0, \dots, 0\rangle. \quad (9)$$

Finally, the electronic population and coherence can be obtained by the construction of the reduced density matrix for electronic motions, which is calculated by the trace of the total density matrix over all nuclear degrees of freedom, i.e.,

$$\rho_{ij}(t) = \text{Tr}_n \{ |\psi_i\rangle \langle \psi_j| \Psi(t) \langle \Psi(t)| \}. \quad (10)$$

C. Computational details

In the current work, the reference geometry of pentacene dimer was directly taken from the previous work,⁸⁹ which is constructed by combining the high-level quantum-chemistry optimized monomer geometry at the ground-state minimum with the TOPAS (the trade name for Ticona cycloolefin copolymers) substrate thin film intermolecular configuration.¹²⁶ The corresponding structure is shown in Fig. 1. The dimer selected here is the pair structure that shows the minimum intermolecular distance in a unit cell, which exhibits relatively large intermolecular electronic coupling. This configuration and similar models, without the surrounding molecules in real crystals, were widely used to study the SF process in pentacene.^{26,86,94,105} Therefore, it is enough to conduct a detailed study on the SF dynamics. The results should give a deep understanding of the mechanism of the SF dynamics of the current stacked pentacene dimer, as well as provide important hints to explore the SF processes in more general stacked configurations.

In order to obtain the vibronic-coupling parameters, the geometry optimization and vibrational analysis of the ground-state minimum for the pentacene monomer were performed at the MP2/CCPV-DZ level using Gaussian 16 software.¹²⁷ This step gave us the frequency and dimensionless normal coordinates of each mode at the ground-state minimum. Then, the gradients of cation, anion, singlet excited, and triplet excited states at the equilibrium

structure of pentacene monomer were calculated with the XMS-CASPT2/CCP-VTZ level using the BAGEL program,¹²⁸ in which the active space of 12 electrons in 12 orbitals was employed, all active orbitals are π and π^* orbitals and three states were averaged to obtain the excited state information.

In the SF dynamics propagation, the initial wave packet at $t = 0$ was directly placed between two LE states ($|\Psi_{S_0 S_1}\rangle$ or $|\Psi_{S_1 S_0}\rangle$), as well as their symmetric or asymmetric combinations ($\frac{1}{\sqrt{2}}[|\Psi_{S_1 S_0}\rangle + |\Psi_{S_0 S_1}\rangle]$ or $-\frac{1}{\sqrt{2}}[|\Psi_{S_1 S_0}\rangle - |\Psi_{S_0 S_1}\rangle]$). The SF quantum dynamics was simulated by the tensor network method with the train structure.

In the current work, all vibrational modes were simply arranged in a line and considered the long-range interactions explicitly, and the MPO was constructed based on previous Refs. 124 and 129. In the convergence test, we compared the SF dynamics results of the full model obtained from the calculations with different modes of ordering, including sorting them by frequencies or randomly. It should be emphasized that the main aim of the current work is to obtain convergent dynamics results and understand the essential characteristics of the SF process by comparing the dynamics of different reduced models; therefore, maximize the computational efficiency was not the core of this study. As shown in Fig. 10 in

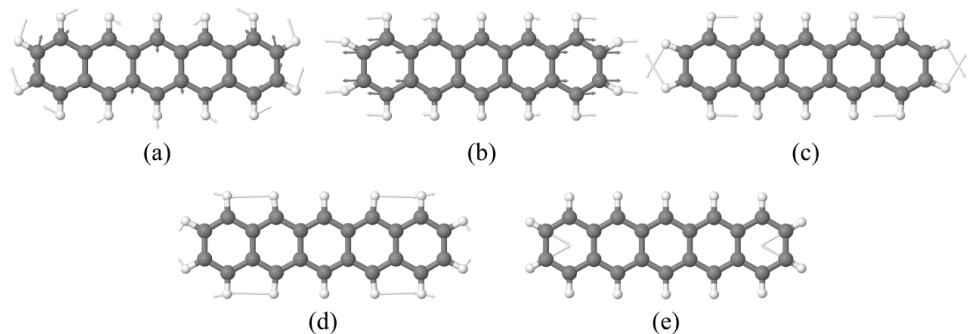


FIG. 3. The vibration directions of some typical normal modes for the pentacene monomer: (a) corresponding to the frequency with 0.014 729 eV; (b) corresponding to the frequency with 0.032 516 eV; (c) corresponding to the frequency with 0.144 957 eV; (d) corresponding to the frequency with 0.149 243 eV; and (e) corresponding to the frequency with 0.401 401 eV.

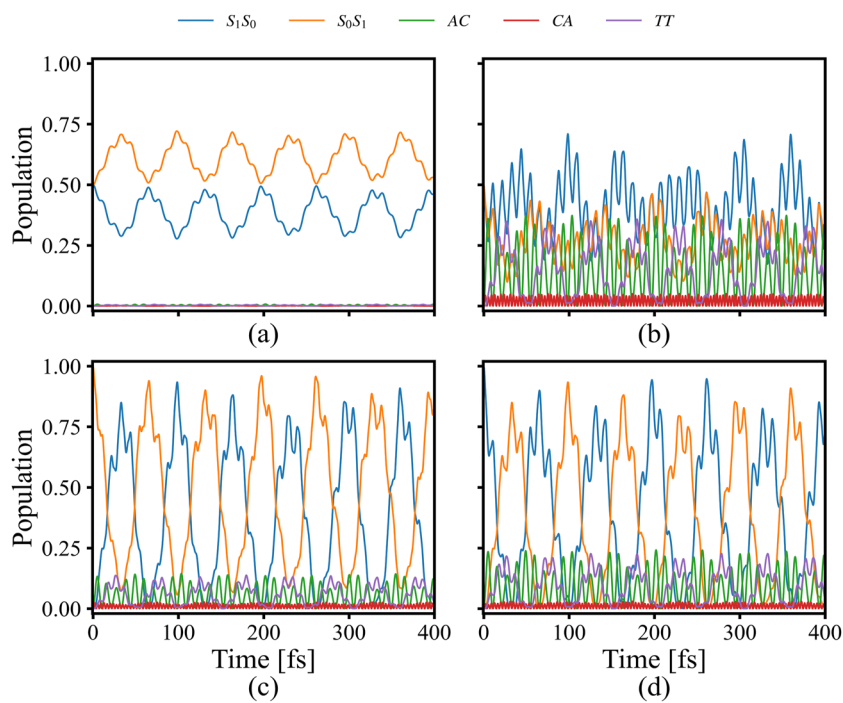


FIG. 4. The time-dependent pure electronic population for different initial states: (a) $-\frac{1}{\sqrt{2}}[|\Psi_{S_1 S_0}\rangle - |\Psi_{S_0 S_1}\rangle]$, (b) $\frac{1}{\sqrt{2}}[|\Psi_{S_1 S_0}\rangle + |\Psi_{S_0 S_1}\rangle]$, (c) $|\Psi_{S_0 S_1}\rangle$, and (d) $|\Psi_{S_1 S_0}\rangle$.

the Appendix, the current SF dynamics is reliable. Certainly, some more advanced approaches, like chain mapping^{130,131} or its extended start-type approach,⁷⁴ may be good choices to further improve the calculation efficiency, especially for complex systems.

To construct the MPS and MPO effectively, the truncation of bond dimension was performed by both dynamical selection via discarding singular values below a fixed cutoff value and fixing the maximal number of retained singular values. The truncated value was set to 10^{-13} for single value decomposition, and the number of basis sets for vibrational modes was obtained by the convergence test. The relevant result is shown in Fig. 11 in the Appendix. Finally, the whole dynamics was evolved to 400 fs with a time step of 0.5 fs based on the one-site TDVP algorithm. In the current work, the number of primitive bases was selected as 15, which should be large enough after some initial tests. When the bond dimension was larger than 60, the convergent dynamics results were achieved in the current simulation time scale. The typical calculation time was close to 59 h on the single Intel Xeon CPU E5-2670 v3 core for the wavepacket propagation of the full model up to 400 fs. The memory requirements were large for the whole simulation, and the relevant machines are configured with a minimum of 64GB of RAM.

III. RESULTS AND DISCUSSION

A. Normal modes and vibronic couplings

For the pentacene monomer, a total of 102 normal modes were obtained from the frequency analysis at the ground-state minimum.

In order to better characterize the importance of different normal modes, Fig. 2 shows the κ/ω values of normal modes for the singlet excited, cationic, anionic, and triplet states of the pentacene monomer. Three groups of molecular vibrations with different frequency domains, <0.05 eV, $0.05\text{--}0.25$ eV, and >0.25 eV, were examined.

As seen, most normal modes with frequencies lower than 0.05 eV display very small $|\kappa|/\omega$ values, which means that the effects of low-frequency normal modes may not be important. Only two low-frequency modes show large vibronic couplings for some electronic states. Figures 3(a) and 3(b) show the vibrational motions of these two normal modes in detail, and the main movement here involves the in-plane stretching and bending motions of the pentacene skeleton.

When the frequency reaches 0.05–0.25 eV, several normal modes exhibit strong vibronic couplings and, therefore, they should

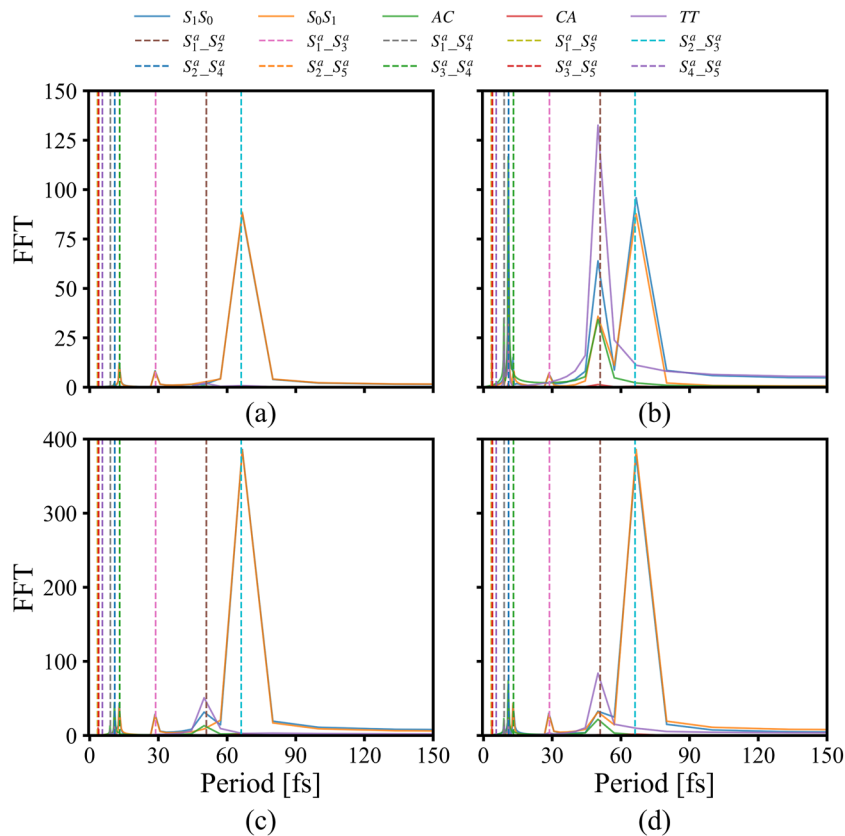


FIG. 5. The FFT of the electronic population for electronic states S_1S_0 , S_0S_1 , electronic AC, CA, and TT for different initial states: (a) $-\frac{1}{\sqrt{2}}[|\Psi_{S_1S_0}\rangle - |\Psi_{S_0S_1}\rangle]$, (b) $\frac{1}{\sqrt{2}}[|\Psi_{S_1S_0}\rangle + |\Psi_{S_0S_1}\rangle]$, (c) $|\Psi_{S_0S_1}\rangle$, and (d) $|\Psi_{S_1S_0}\rangle$. The vertical dashed lines represent the vibrational frequency corresponding to the adiabatic energy difference between every two states.

have a significant impact on the nonadiabatic SF dynamics. In addition, the vibrations of two typical normal modes within this frequency range are collected in Figs. 3(c) and 3(d), in which the change of the skeleton is also the leading way of movement. Particularly, most modes with strong vibronic coupling are relevant to the CC bond stretching motions. The reason is easily understood. Here, all involved states display the $\pi\pi^*$ characters. The CC bond stretching motion can modify the conjugated statuses, changing the energies of the π and π^* orbitals. As a consequence, the $\pi\pi^*$ state energy is highly dependent on the CC bond lengths. Therefore, these modes display strong vibronic couplings.

The remaining high-frequency normal modes with a frequency larger than 0.25 eV exhibit small $|\kappa|/\omega$ values, and the main motion is the in-plane stretching motion of the carbon–hydrogen bond, as shown in Fig. 3(e). Since the CH distances have little influence on the conjugated statuses and, therefore, do not modify the energies of the $\pi\pi^*$ states, these modes display small vibronic couplings.

B. Pure electronic dynamics

Then, we consider the pure electronic dynamics without the vibrational degrees of freedom. Although such dynamics in principle are rather simple, we still prefer to start our discussion with them because the careful analyses of these data may display some deep physical insights to help further understand true nonadiabatic SF dynamics.

The pure electronic dynamics starting from different initial conditions are shown in Fig. 4, in which the obvious population transfer occurs among different diabatic electronic states. As expected, the oscillation appears in the population dynamics, which reflects the quantum coherence in the pure electronic dynamics. In

fact, starting from different initial conditions, the population transfer dynamics here show different patterns. When the initial state is $-\frac{1}{\sqrt{2}}[|\Psi_{S_1S_0}\rangle - |\Psi_{S_0S_1}\rangle]$, a small amplitude population oscillation is observed, and the oscillation period is rather long with respect to other cases. When the initial state is $|\Psi_{S_0S_1}\rangle$ or $|\Psi_{S_1S_0}\rangle$, the oscillation in the population becomes significant, indicating the fast population transfer between two LE states. When the initial state $-\frac{1}{\sqrt{2}}[|\Psi_{S_1S_0}\rangle + |\Psi_{S_0S_1}\rangle]$ is prepared, we notice that high-frequency oscillations appear in the population dynamics and many states are populated. These results indicate that a full understanding of pure electronic dynamics is not trivial. For further analysis, we performed the fast Fourier transform (FFT) on the time-dependent population, and the diabatic-to-adiabatic transformation matrix of the electronic Hamiltonian was checked to explain some interesting features. The concrete results are summarized in Figs. 5 and 6.

For the initial state with $-\frac{1}{\sqrt{2}}[|\Psi_{S_1S_0}\rangle - |\Psi_{S_0S_1}\rangle]$, the dynamics is basically characterized by the coincident population oscillation between two LE states, while other states seem not to be populated. The overall oscillation patterns appear very simple in the population dynamics. The FFT analyses show that the position of the highest peak approximates 66.67 fs, which corresponds to the oscillation frequency with the energy difference between adiabatic electronic states S_2^a and S_3^a . This phenomenon can also be understood in terms of the diabatic-to-adiabatic transformation matrix shown in Fig. 6, where both S_2^a and S_3^a states have larger weights. Although, at first glance, the quantum dynamics here seems to only involve two LE states, other states are not relevant at all. However, this is not true since such oscillation cannot be the simple Rabi-type oscillation between two LE states due to their extremely weak coupling (-0.006 eV). Instead, this population transfer process is fully governed by the super-exchange mechanism mediated by the

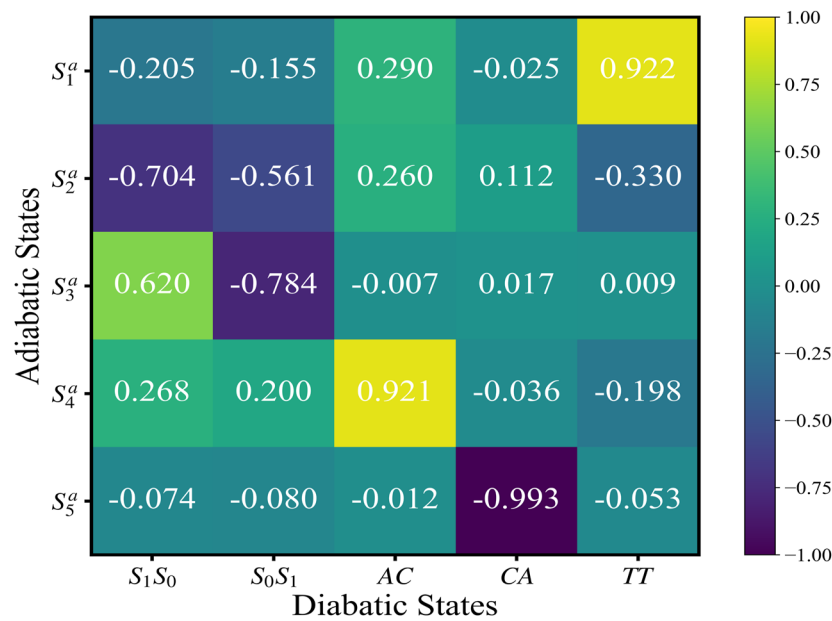


FIG. 6. The heatmap of the transformation matrix between diabatic and adiabatic electronic states.

CT state, in which the *AC* state is not far from two *LE* states and also displays the visible *AC-LE* couplings. This idea is supported by the existence of another two relatively significant peaks at 10.00 and 30.00 fs in the FFT analysis of the population dynamics, which result from the $S_1^a - S_3^a$ and $S_3^a - S_4^a$ energy differences, respectively. Here, the S_4^a state is mainly characterized by the *AC* component according to the diabatic-to-adiabatic transformation matrix.

However, for the other three cases with $\frac{1}{\sqrt{2}}[|\Psi_{S_1S_0}\rangle + |\Psi_{S_0S_1}\rangle]$, $|\Psi_{S_0S_1}\rangle$ or $|\Psi_{S_1S_0}\rangle$ as the initial state, the more significant population transfer and large oscillations appear in the population dynamics. The high-frequency components appear in all these cases. The *AC* state and even the *TT* state are populated during the electronic dynamics. After the FFT analysis of the electronic populations vs time, three peaks are found at the same locations, which are similar to those in the dynamics from the first initial condition with $-\frac{1}{\sqrt{2}}[|\Psi_{S_1S_0}\rangle - |\Psi_{S_0S_1}\rangle]$. In addition, several additional peaks were discovered, near 3.85, 9.00, 50.00 fs, which correspond to the $S_3^a - S_5^a$, $S_1^a - S_4^a$, and $S_1^a - S_2^a$ energy differences, respectively. This indicates that two *LE* components, *AC* and *TT*, are involved, while the *CA* component does not play an essential role.

According to the electronic Hamiltonian, the *LE-LE* coupling is rather weak and the *LE-TT* coupling is even negligible, while the *LE-AC* and *AC-TT* couplings are visible. Therefore, we believed that the *AC* state is very important here, which not only bridges the *LE-LE* state population transfer but also the *LE-TT* population transfer. Since the energy of the *AC* state is higher than that of the

LE and *TT* states, the excited-state energy transfer and the SF processes are governed by the super-exchanging mechanism in the pure electronic dynamics. The *TT* state can be formed via the *AC* state due to the pronounced *AC-TT* coupling instead of the direct pathway. The *CA* state seems unimportant because of its higher energy. This again shows that the asymmetrical configuration of the stacked dimer has the potential to influence the final SF dynamics because such a feature causes different energies in two *CT* states.

One central question is why different population dynamics exist for different initial conditions, particularly for the symmetric or asymmetric combination of two *LE* states. The underlying reason is as follows. Two *LE-AC* couplings display the same sign. When we consider the symmetric and asymmetric combinations of two *LE* states, the resulting state should show large and small electronic couplings with the *AC* state, respectively. As a consequence, we should only see the significant and weak population transfer between the symmetric and asymmetric combinations of two *LE* states and one *AC* state, respectively. This explains why different oscillation patterns exist in the population dynamics with different initial conditions. In addition, in the $\frac{1}{\sqrt{2}}[|\Psi_{S_1S_0}\rangle + |\Psi_{S_0S_1}\rangle]$ situation, the *TT* state can be easily formed due to the deep involvement of the *CT* state in the quantum dynamics. When the dynamics starts in one of the *LE* states, the population transfer takes place between two *LE* states due to the *CT*-mediated exchanging mechanism, as discussed earlier. As the *AC* state is involved, we also observed the minor formation of the *TT* state.

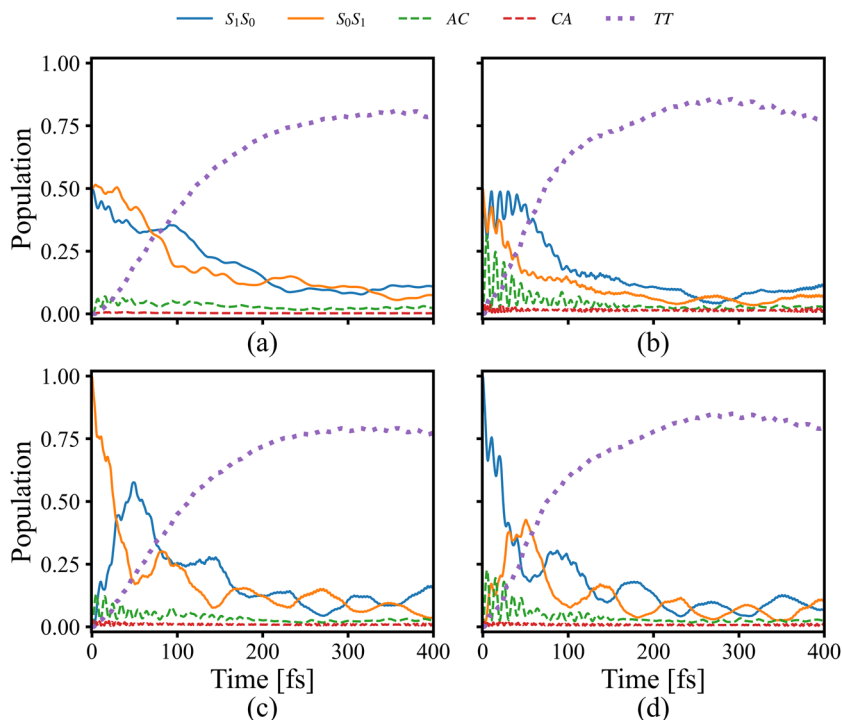


FIG. 7. The time-dependent electronic populations of the electronic states S_1S_0 , S_0S_1 , *AC*, *CA*, and *TT* with different initial conditions: (a) $-\frac{1}{\sqrt{2}}[|\Psi_{S_1S_0}\rangle - |\Psi_{S_0S_1}\rangle]$, (b) $\frac{1}{\sqrt{2}}[|\Psi_{S_1S_0}\rangle + |\Psi_{S_0S_1}\rangle]$, (c) $|\Psi_{S_0S_1}\rangle$, and (d) $|\Psi_{S_1S_0}\rangle$.

C. Singlet fission dynamics

As the pentacene monomer displays the C_{2V} symmetry, in principle only the A_1 modes of each monomer should display the visible linear vibronic coupling terms due to the symmetry selection rule. Therefore, the vibrational modes with strong intrastate vibronic coupling here should be the A_1 modes that can modify the energy of the $\pi-\pi^*$ transitions. In the projection of the gradient, we also find the modes with other symmetries display very minor coupling strengths. Therefore, in the below discussions, we start with the diabatic model with all A_1 modes (18 modes for each monomer and a total of 36 modes for the dimer). Figure 7 shows the SF dynamics with the inclusion of all effectively vibrational degrees of freedom from different initial states, in which the time-dependent electronic population exhibits a qualitatively consistent decay pattern. Initially, the population of the LE state decays rapidly in all situations. Simultaneously, the CT state is instantaneously activated, then the population transfer occurs between the LE and CT states, especially for the initial states with $\frac{1}{\sqrt{2}}[|\Psi_{S_1S_0}\rangle + |\Psi_{S_0S_1}\rangle]$, $|\Psi_{S_0S_1}\rangle$, and $|\Psi_{S_1S_0}\rangle$. While throughout the whole dynamics process, the TT -state population is increased almost exponentially with the fitted rate constants 120, 70, 106, and 77 fs, respectively, which are close to the previous experimental and theoretical observations.⁹³ Since the $LE-TT$ coupling is extremely weak in the current model, the ultrafast SF process is only possible via the CT -mediated mechanism, which was also confirmed in the previous studies on the pentacene and derivative.^{74,85,114}

Similar to the pure electronic dynamics, both AC and CA states play different roles in the whole SF process. Because the CA state lies in a very high energy domain, it is not populated in the SF dynamics. As a contrast, the population of the AC state is visible, especially when the initial state is formed by two LE states or their symmetric combination. Besides, the AC state also displays the obvious population transfer with high oscillation patterns in the early stage of dynamics, as shown in Fig. 7. As the symmetric combination of two LE states may define strong $LE-CT$ couplings, a larger CT population exists in symmetric combination situations. As a consequence, the formation of the TT state is also slightly faster in this case. The reversed situation is given by the asymmetric combination of two LE states.

In order to further understand the observations earlier, two reduced four-state models were constructed based on the original model Hamiltonian with the initial state $\frac{1}{\sqrt{2}}[|\Psi_{S_1S_0}\rangle + |\Psi_{S_0S_1}\rangle]$ so that the effect of the CT state can be analyzed in detail. Here, we either discarded the CA or AC state to define two four-state models. Figure 12 in the Appendix shows the corresponding time-dependent populations of these reduced four-state models. It can be seen that when only the AC state was considered, the overall dynamics pattern obtained here is quite similar to the original five-state results, although the time-dependent population of electronic state TT is slightly overestimated. For the second four-state model with the CA state included, the dynamics results are different, and the population transfer to the TT state becomes much slower. Therefore, the

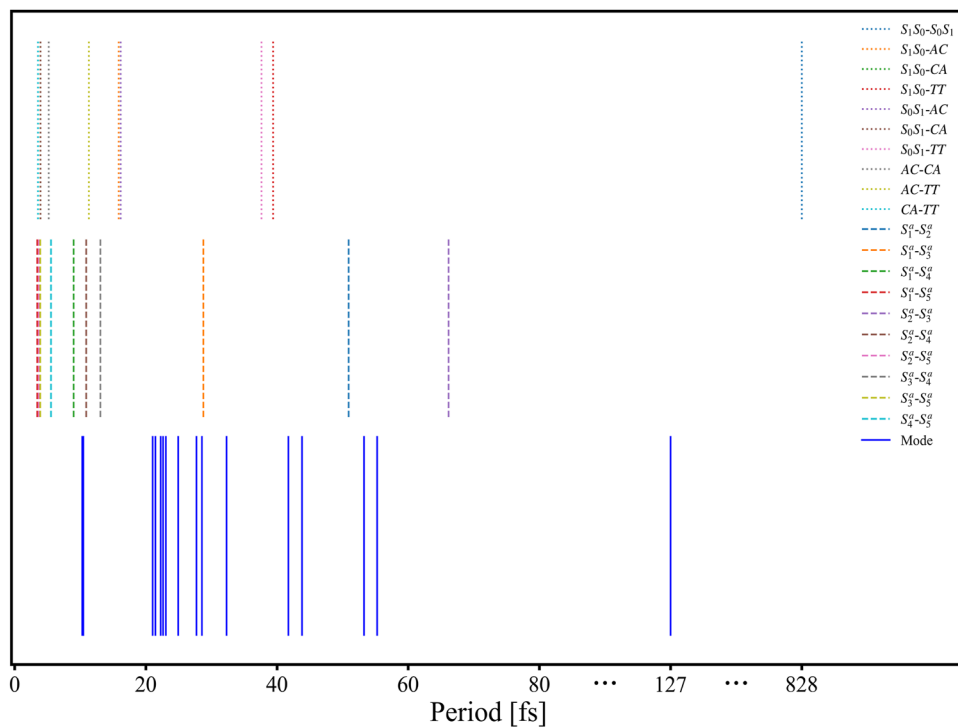


FIG. 8. The vibrational period involved in the reduced model: the blue lines denote the vibrational periods of reserved modes; the dashed lines denote the oscillation period corresponding to energy differences between adiabatic states; and the dotted lines denote the oscillation period corresponding to energy differences between diabatic states.

conclusion can be further supported by the fact that the AC and CA states may play different roles in the population transfer of electronic state *TT*. In addition, this phenomenon also appears in the pentacene derivative.⁷⁴ Overall, the SF dynamics is prone to follow the population transfer from the *LE* state to the multi-exciton *TT* one, which is the typical characteristic of the super-exchange mechanism.

It is noticeable that the quantum yield only reaches 75% up to the current simulation time scale (400 fs). This inconsistency with respect to some previous works^{74,93} is very interesting. The underlined reasons are very complex and may be understood in the following ways. Experimentally, the research target is condensed material systems. Compared with the experimental conditions, the

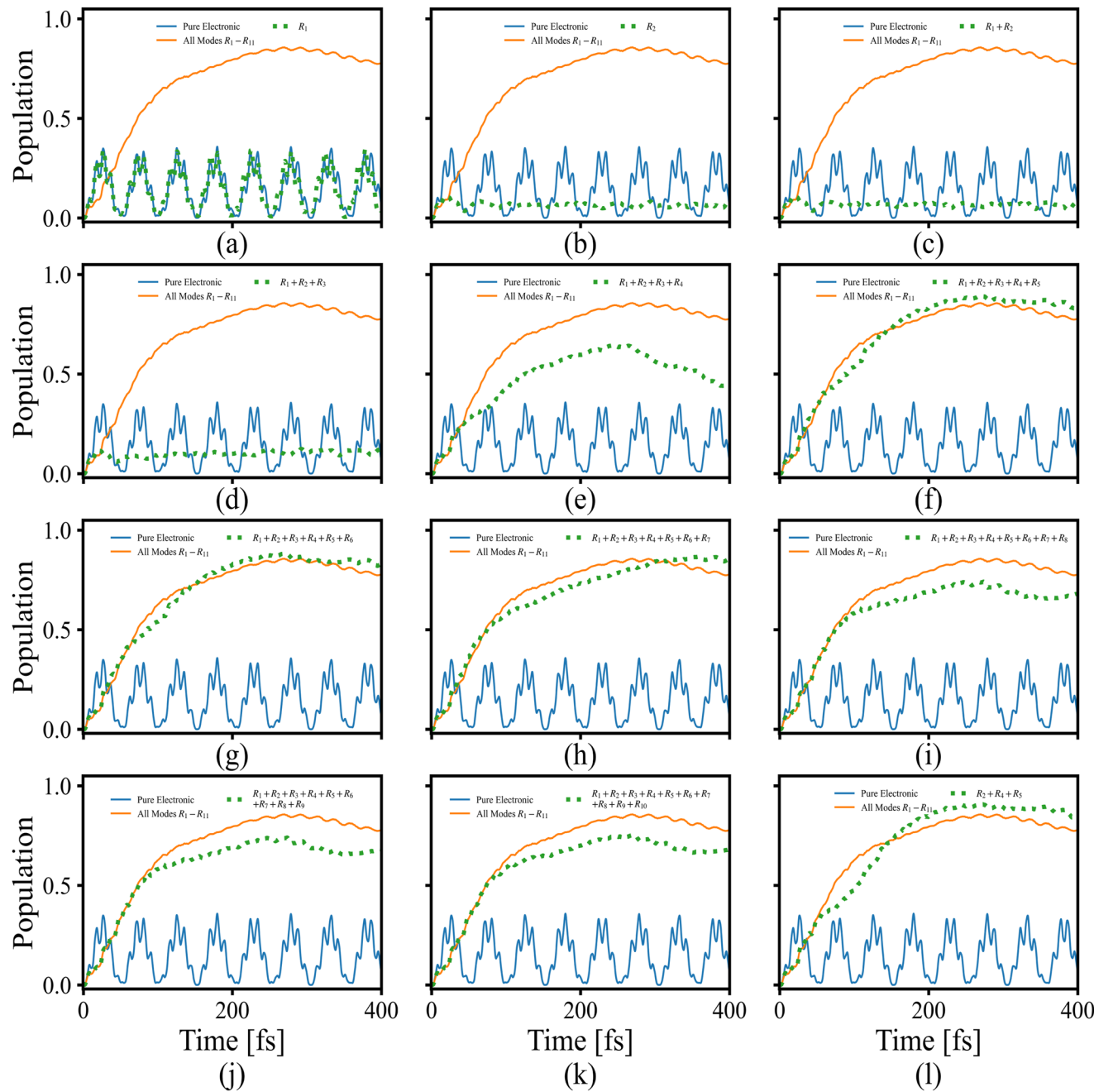


FIG. 9. The time-dependent population of electronic state *TT* based on the initial state $\frac{1}{\sqrt{2}}[|\Psi_{S_1S_0}\rangle + |\Psi_{S_0S_1}\rangle]$ with modes in different regions, in which the modes were combined sequentially in accordance with the period from small to large.

current work employed a simplified dimer model in which only the intramolecular coupling was considered. Therefore, the missing description of the condensed matter systems and other potential factors certainly have some potential impacts on the quantum yield of the SF dynamics. Theoretically, not all previous works gave 100% quantum yields within the time scale of 400 fs. Some previous works^{60,109,114,132} show a similar quantum yield (75%). However, other theoretical works show that the quantum yield can exceed more than 90% or even reach 100%.^{74,93} As these works employed different Hamiltonian models constructed at various quantum-chemistry levels and simulated the quantum dynamics using different dynamics methods, it is not very transparent to give the precise reasons for these inconsistencies. For the current diabatic model Hamiltonian, it is definite that both the interstate couplings

(off-diagonal elements) and energy (diagonal elements) differences between any two states are smaller than their corresponding values given in some previous work,⁹³ which means that the later case results in an easier conversion from *LE* to *TT* states in principle. This may partially explain the different quantum yields among these works, while it is hard to determine whether the inconsistency is fully due to the different chosen quantum chemistry methods or not.

Besides, it is also important to note that the oscillation patterns of the population evolution in the early stage of the SF dynamics is comparable to the pure electronic dynamics without the consideration of vibrational degrees of freedom, which demonstrates the dominant process at this stage involves the population interchange between the S_1S_0 and S_0S_1 states mediated by the CT one, and the vibrational degrees of freedom here have little impact on the early

TABLE II. The parameters of frequencies and the electronic–phonon couplings (in eV) for all A_1 modes.

Frequency	S_1S_0	S_0S_1	AC	CA	TT
0.032 516	-0.015 686	0.000 000	-0.028 929	0.014 225	-0.013 981
0.074 878	0.007 802	0.000 000	0.018 566	-0.012 140	0.009 755
0.077 694	-0.006 104	0.000 000	-0.005 746	-0.000 797	-0.000 511
0.094 445	-0.050 825	0.000 000	-0.028 576	-0.016 968	-0.043 225
0.099 183	-0.007 636	0.000 000	-0.020 361	-0.011 362	-0.030 902
0.128 104	0.025 348	0.000 000	0.020 311	0.022 932	0.021 080
0.144 957	-0.042 922	0.000 000	-0.023 447	-0.015 052	-0.050 176
0.149 243	0.051 825	0.000 000	0.032 766	0.034 232	0.082 734
0.166 037	0.043 884	0.000 000	0.023 269	0.023 148	-0.029 459
0.179 442	-0.086 685	0.000 000	-0.057 275	-0.041 311	-0.098 372
0.182 880	0.056 013	0.000 000	0.031 587	0.016 630	0.127 282
0.182 919	0.019 303	0.000 000	-0.000 000	0.000 000	-0.000 000
0.185 854	0.024 438	0.000 000	0.014 207	0.014 684	-0.041 824
0.192 871	-0.086 619	0.000 000	-0.018 448	-0.061 165	-0.146 108
0.196 718	0.027 400	0.000 000	0.001 095	0.012 696	-0.045 782
0.395 757	-0.008 727	0.000 000	-0.013 256	-0.025 695	-0.016 480
0.397 594	-0.008 275	0.000 000	0.001 241	-0.014 583	-0.008 516
0.401 401	-0.017 255	0.000 000	0.000 943	-0.021 579	-0.017 810
0.032 516	0.000 000	-0.015 686	0.014 225	-0.028 929	-0.013 981
0.074 878	0.000 000	0.007 802	-0.012 140	0.018 566	0.009 755
0.077 694	-0.006 104	0.000 000	-0.005 746	-0.000 797	-0.000 511
0.094 445	0.000 000	-0.050 825	-0.016 968	-0.028 576	-0.043 225
0.099 183	0.000 000	-0.007 636	-0.011 362	-0.020 361	-0.030 902
0.128 104	0.000 000	0.025 348	0.022 932	0.020 311	0.021 080
0.144 957	0.000 000	-0.042 922	-0.015 052	-0.023 447	-0.050 176
0.149 243	0.000 000	0.051 825	0.034 232	0.032 766	0.082 734
0.166 037	0.000 000	0.043 884	0.023 148	0.023 269	-0.029 459
0.179 442	0.000 000	-0.086 685	-0.041 311	-0.057 275	-0.098 372
0.182 880	0.000 000	0.056 013	0.016 630	0.031 587	0.127 282
0.182 919	0.000 000	0.019 303	0.000 000	-0.000 000	-0.000 000
0.185 854	0.000 000	0.024 438	0.014 684	0.014 207	-0.041 824
0.192 871	0.000 000	-0.086 619	-0.061 165	-0.018 448	-0.146 108
0.196 718	0.000 000	0.027 400	0.012 696	0.001 095	-0.045 782
0.395 757	0.000 000	-0.008 727	-0.025 695	-0.013 256	-0.016 480
0.397 594	0.000 000	-0.008 275	-0.014 583	0.001 241	-0.008 516
0.401 401	0.000 000	-0.017 255	-0.021 579	0.000 943	-0.017 810

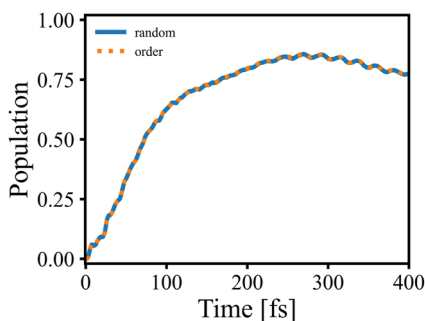


FIG. 10. The dynamics results under different modes of ordering: the blue line denotes random ordering; the orange dotted line represents the sorting by the vibration frequency.

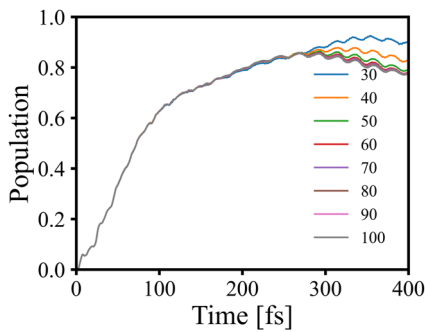


FIG. 11. The convergence test based on the bond dimension.

stage dynamics. A similar phenomenon was also found in the previous study of the pentacene derivative.⁷⁴ While with time evolution, the population transfer from the S_1S_0 to S_0S_1 state appears to be suppressed by the vibrational degrees of freedom involved due to the strong vibronic coupling effects. From this point of view, a natural question would be raised about how different vibrational degrees of freedom influence the electronic dynamics. This problem was

noticed by several groups in their previous studies on the relevant topic.^{74,114}

In order to further understand the role of the vibrational degree of freedom in the SF dynamics, a series of reduced dimensional Hamiltonians were considered on the basis of the original model. Then, the contribution of different vibrational modes was investigated in terms of these reduced dimensional Hamiltonians.

In light of the similarities among the SF dynamics patterns earlier, only the case with the initial state $\frac{1}{\sqrt{2}}(|\Psi_{S_1S_0}\rangle + |\Psi_{S_0S_1}\rangle)$ was selected as the prototype for further studies in order to simplify the problem itself and avoid excessive computations.

Figure 8 exhibits the vibrational period of each selected mode. According to this particular distribution, the chosen modes were further divided into 11 parts (R_1-R_{11}) in the following analysis. Therein, the region R_1 contains the modes with vibrational frequencies less than 20 fs, the region R_2 includes the modes with vibrational frequencies between 20 and 24 fs, and the remaining modes with vibrational frequencies larger than 24 fs are sequentially named as the regions R_3-R_{11} in accordance with the period from small to large, where each region only contains one vibrational mode for each monomer. Then, the vibrational modes in different regions were successively considered or combined to perform dynamics calculations. The corresponding population results of the TT state over time are summarized in Fig. 9.

When only the region R_1 (total eight modes with a frequency of 0.397 594–0.401 401 eV) is considered, where the primary motions here involve the stretching motions of the carbon–hydrogen bond as shown in Fig. 3(e), the simulated population is quite similar to the pure electronic observation, and the TT population oscillates vs time. This indicates that the high-frequency modes or the relative vibrations of carbon–hydrogen bonds have a minor effect on the pure electronic transition, especially in the early stage of dynamics. The underlying reason may consist of two facts: on the one hand, these high-frequency modes are too far from the resonance of the electronic transition (especially from the purple dashed line shown in the middle part of Fig. 8); on the other hand, their vibronic couplings are very small, as shown in Fig. 13 of the Appendix.

However, when the region R_2 (total ten modes with a frequency of 0.179 442–0.196 718 eV) was used to perform dynamics

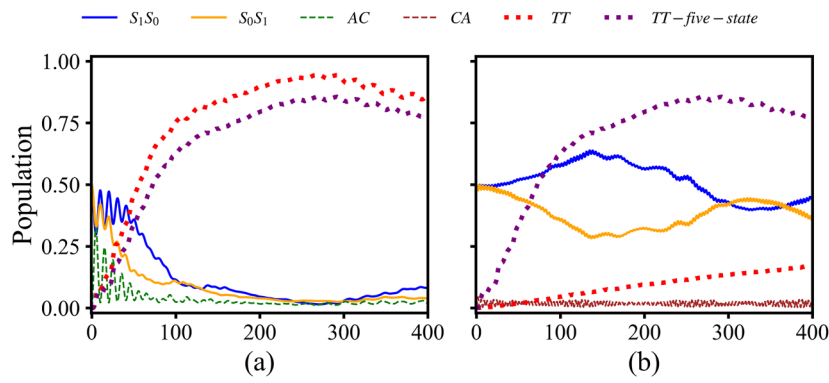


FIG. 12. The time-dependent population of reduced four-state model: (a) only the charge-transfer state AC was considered; (b) only the charge-transfer state CA was included.

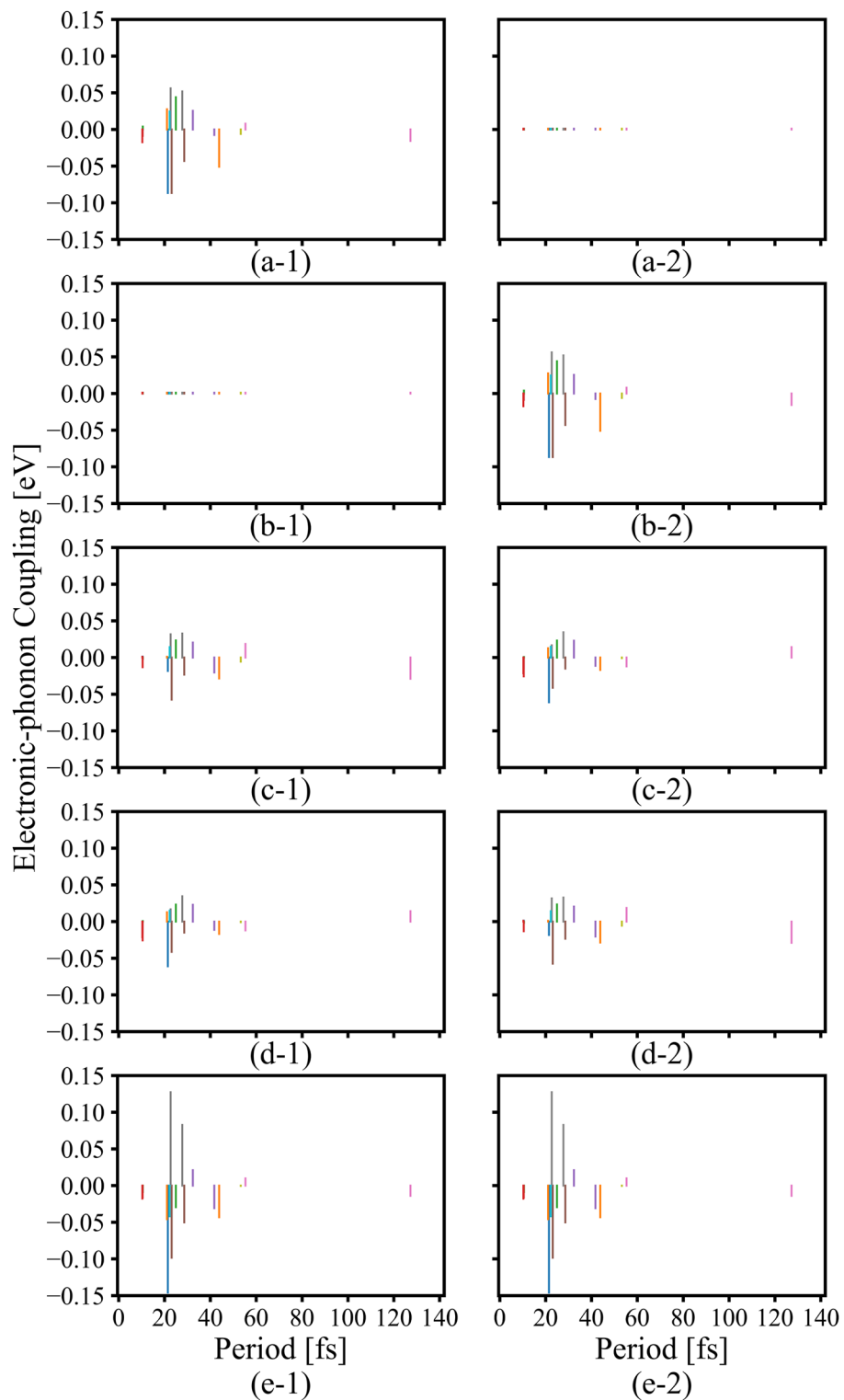


FIG. 13. The electronic–phonon coupling of different reserved modes. (a)–(d) correspond to the modes coupled to the S_1S_0 , S_0S_1 , AC, CA, and TT, respectively. 1 and 2 denote the modes related to different monomers.

simulation, a completely different feature is exhibited in Fig. 9. The dynamics here indicates that the vibrational modes in the region R_2 can damp the electronic oscillation; therefore, the population of the electronic state TT becomes flat and stable. This may be due to the fact that the vibronic coupling in this region is much larger and more widely distributed, as shown in Fig. 13 of the Appendix, and the dominant vibration modes here are the changes in the pentacene skeleton.

On this basis, when combining two regions, R_1 and R_2 , only the dynamics pattern appeared in the region R_2 . In addition, an analogous time-dependent population of electronic state TT was obtained when the region R_3 (total of two modes with a frequency of 0.166 037 eV) was included. This indicates that the modes in the R_3 region do not show other effects as compared to the ones in the R_2 region.

Interestingly, when the region R_4 (total of two modes with a frequency of 0.149 243 eV) was added to the above-mentioned combination, the dynamics pattern changed significantly, in which the time-dependent population of the TT state began to approach the original dynamics results, although the population is underestimated. In addition, this deviation can be greatly alleviated with the involvement of modes in region R_5 (total of two modes with a frequency of 0.144 957 eV), and the time-dependent population of the TT state is very close to the results of the high-dimensional model Hamiltonian.

Therefore, the modes in regions of R_4 and R_5 have great influences on dynamics. The detailed reasons can be easily understood in the adiabatic picture. The modes in R_4 and R_5 regions are resonant to the oscillation period corresponding to the energy difference between adiabatic states S_1^a and S_3^a , whose leading movements are the change of the skeleton, as shown in Figs. 3(c) and 3(d).

As for other regions (R_6-R_{11}), the relevant modes involved only play a role in fine-tuning of dynamics results, as shown in Fig. 9. Their minor influence can be explained by their weak vibronic couplings and their low frequencies, far from those for electronic transitions.

D. Discussion

In the current work, the model constructed therein combines the data from two different high-level electronic structure calculations. Such a choice is mainly due to the complexity of the construction of the diabatic model. However, we still believe that the current setup is reasonable. On the one hand, the electronic Hamiltonian matrix should be accurate enough since it is constructed at the XMC-QDPT level. On the other hand, the electronic states included in the current systems are mainly $\pi\pi^*$ states, and the electronic transitions involve frontier orbitals of π and π^* . In this case, only if some vibrational modes can modify the energies of π and π^* orbitals, and their interstate vibronic couplings should be strong. In principle, such types of modes should be relevant to the stretching motion of the carbon–carbon bond in the current system. Therefore, even if the vibronic coupling values may depend on the electronic methods used, their major features should be similar, i.e., the important modes and the amplitudes of their vibronic couplings should not be far from each other. In this sense, even though these numbers change slightly, we can still obtain the dynamics features, which are not far from the current results. Therefore, our current model makes it reasonable to conduct studies on the SF dynamics.

One weak point is that the vibrational modes of the monomer were employed to build the vibronic coupling modes. This may bring some bias. For instance, the monomer shows the C_{2v} symmetry and, therefore, only the A_1 modes should show the intrastate linear vibronic coupling here. In stacked systems, such symmetry does not strictly remain and, therefore, the symmetry selection rule should not be followed. However, we expect that the geometrical distortion should be small. In addition, the modes that can modify the $\pi-\pi^*$ transitions should still be very important here. As a consequence, we expect that the intramolecular modes that show strong vibronic coupling should be similar in the monomer and stacked systems. However, the monomer-based approaches may find it hard to capture the long-range intermolecular vibrations that lead to the strong fluctuations of the intermolecular couplings between neighboring monomers. However, for the current pentacene dimer system, the SF process occurs within a very short time scale after initial photoexcitation. As the motion of long-range vibrations is usually slow, they should not be in resonance with the electronic dynamics due to different time scales. Therefore, the local intramolecular vibrational modes were considered to build the SF model. The dynamics results and analyses also further validate the effectiveness of such considerations, in which the SF process occurs on an ultrafast time scale and the modes with low frequencies do not resonate with the electronic vibrations. Certainly, we should realize that long-range vibrations may be important for the electronic structure and dynamics in certain cases¹³³ where the delocalized electrons interact more strongly with thermally activated low-frequency vibrations. To describe such phenomena, the low-frequency mode should be explicitly considered, and they may be treated with the consideration of static disorder in future work.

There is no doubt that the SF process is very complex; therefore, more efforts are needed to further explore the details of the dynamics. For example, temperature and environmental effects are all important and challenging topics in this field. It is worth noting that some previous works have made prospective explorations, which provide ideas for further detailed research.

For the temperature, some results^{84,86,95,97,114} show that the thermal effect tends to excite the low-frequency mode and does not have impacts on the high-frequency one. Our previous work has also demonstrated that the temperature effect does not have a decisive effect on the SF process for a specific time scale.¹¹⁴ The reason involved is very simple: the motions of these low-frequency modes show different time scales with respect to the ultrafast SF dynamics. However, it should be acknowledged that the low-frequency mode may become more and more important as the SF dynamics become slower. To consider such effects, the combination of the tensor network method and the thermo-field theories may be a good choice.¹³⁴

The crystal environment usually involves different packing statuses and more complex states. The studies on them should be challenging because the corresponding effect is more complicated and highly system dependent.⁸⁸ For instance, the previous works^{84,88,133} show the strong mixing of the LE and CT characters in the adiabatic excited states in the crystal phase, which may deeply modify the mechanism of the SF dynamics. Although these studies provide primary understandings on this topic, many problems remain unsolved, and we still need to think about how to build a suitable

model to describe the crystal effects and how to simulate the SF dynamics process with a huge number of molecules.

Recently, we also noticed that other prospecting efforts have been taken into the construction of the SF Hamiltonian, in which the coupling between *LE* and *TT* states was further considered, and the SF process was considered in terms of the conical intersection between the singlet exciton and triplet-pair states.⁹⁴ Therefore, it would be very interesting to add the conical intersection directly to the model and check the dynamics performance.

IV. CONCLUSION

In this paper, we focus our efforts on the rather accurate and detailed investigation of the SF process in the stacked polyacene dimer by combining electronic-structure calculations and quantum dynamics simulations. On the basis of the electronic Hamiltonian derived from the previous high-level quantum chemistry method, the vibronic coupling parameters were calculated by ourselves to construct the linear vibronic coupling model. Then, the tensor network method with high efficiency and great potential was used to study the quantum propagation of the SF process and explore the influence of different factors.

The model Hamiltonian in this work contains five electronic states (two *LE*, two *CT*, and one *TT*) and a bunch of vibrational modes. The frequency analysis shows that several in-plane CC stretching vibrational modes exhibit strong vibronic couplings because they can significantly modify the $\pi-\pi^*$ transitions, which have significant impacts on the nonadiabatic SF dynamics.

The pure electronic dynamics provides some preliminary but important perspectives to understand the SF process. The results indicate that the population transfer dynamics display dissimilar patterns when starting from different initial conditions. The frequency-domain analyses of the population dynamics reveal that the periods of the oscillations of electronic populations are relevant to the energy gap between different adiabatic states. The population transfer between two *LE* states is fully governed by the super-exchange mechanism mediated by the *CT* state, and even the *TT* state can be populated during the electronic dynamics. The symmetric or asymmetric linear combination of two *LE* states results in different population dynamics because of the quantum superposition. These phenomena mean that the electronic Hamiltonian itself contains all possible “reaction pathways.” Therefore, the pure electronic dynamics analysis can be used as a useful beginning for the exploration of the complex nonadiabatic process.

The current SF dynamics are close to the earlier experimental and theoretical observations, which supports the *CT*-mediated mechanism in the pentacene dimer. For the current five-state model, one of the *CT* states (*AC*) plays an important role in the SF dynamics due to the lower energy, and the super-exchanging mechanism is governed by this state. The introduction of the vibrational degrees of freedom would enhance the probability towards the “reaction channel” from *LE* to *TT* mediated by *CT*. However, different roles for the vibrational modes were found. Some modes with frequencies far from the quantum resonance of the electronic transitions or with very minor vibronic couplings are basically bystander modes. A few modes show the frequency resonance with the adiabatic energy gap, which drives the ultrafast SF dynamics. The other modes add damping effects to the SF dynamics.

Overall, the current work provides a deep and detailed understanding of the SF process in the pentacene dimer. In addition, it also verifies the efficiency of the tensor network method with the train structure in the treatment of the quantum dynamics for complex systems. This can serve as a reference for other similar systems to study and explore dynamic behaviors. Besides, time-resolved spectroscopy is often used in the study of SF processes. The spectral simulation is very important to provide some new perspectives to understand experimental observations. This should be an important topic in the future.

ACKNOWLEDGMENTS

This work is supported by NSFC projects (Grant Nos. 21933011, 22333003, 21873112, and 22173107) and the Opening Project of the Key Laboratory of Optoelectronic Chemical Materials and Devices of the Ministry of Education, Jianghan University (Grant No. JDGD-202216). The authors acknowledge the Supercomputing Center, Computer Network Information Center, Chinese Academy of Sciences, and the National Supercomputing Center in Shenzhen for providing computational resources.

AUTHOR DECLARATIONS

Conflict of Interest

The authors have no conflicts to disclose.

Author Contributions

Jiawei Peng: Conceptualization (equal); Data curation (equal); Formal analysis (equal); Investigation (lead); Methodology (equal); Software (equal); Validation (equal); Visualization (equal); Writing – original draft (lead); Writing – review & editing (equal). **Deping Hu:** Investigation (supporting); Methodology (supporting); Validation (equal). **Hong Liu:** Conceptualization (equal); Project administration (supporting); Resources (supporting); Supervision (supporting). **Qiang Shi:** Formal analysis (supporting); Methodology (supporting); Software (supporting); Writing – review & editing (equal). **Peng Bao:** Funding acquisition (equal); Methodology (equal); Software (supporting); Writing – review & editing (equal). **Zhenggang Lan:** Conceptualization (equal); Formal analysis (equal); Funding acquisition (equal); Investigation (equal); Methodology (equal); Project administration (lead); Resources (equal); Supervision (lead); Visualization (equal); Writing – original draft (equal); Writing – review & editing (lead).

DATA AVAILABILITY

The data and code that support the findings of this study are available from the corresponding author upon reasonable request.

APPENDIX: MODEL PARAMETERS

The parameters V_{kl} in the molecular Hamiltonian (in eV) were given in Table I. The parameters of frequencies and the electronic-phonon couplings (in eV) for all A_1 modes were given in Table II.

REFERENCES

- ¹A. Muller, Y. Avlasevich, K. Mullen, and C. Bardeen, "Evidence for exciton fission and fusion in a covalently linked tetracene dimer," *Chem. Phys. Lett.* **421**, 518–522 (2006).
- ²J. Zirzlmeier, D. Lehnher, P. B. Coto, E. T. Chernick, R. Casillas, B. S. Basel, M. Thoss, R. R. Tykwiński, and D. M. Guldi, "Singlet fission in pentacene dimers," *Proc. Natl. Acad. Sci. U. S. A.* **112**, 5325–5330 (2015).
- ³J. N. Schrauben, A. Akdag, J. Wen, Z. Havlas, J. L. Ryerson, M. B. Smith, J. Michl, and J. C. Johnson, "Excitation localization/delocalization isomerism in a strongly coupled covalent dimer of 1,3-diphenylisobenzofuran," *J. Phys. Chem. A* **120**, 3473–3483 (2016).
- ⁴O. Varnavski, N. Abeyasinghe, J. Arago, J. J. Serrano-Perez, E. Ortí, J. T. Lopez Navarrete, K. Takimiya, D. Casanova, J. Casado, and T. Goodson, "High yield ultrafast intramolecular singlet exciton fission in a quinoidal bithiophene," *J. Phys. Chem. Lett.* **6**, 1375–1384 (2015).
- ⁵E. A. Margulies, C. E. Miller, Y. Wu, L. Ma, G. C. Schatz, R. M. Young, and M. R. Wasielewski, "Enabling singlet fission by controlling intramolecular charge transfer in π -stacked covalent terrylenediimide dimers," *Nat. Chem.* **8**, 1120–1125 (2016).
- ⁶T. Zeng and P. Goel, "Design of small intramolecular singlet fission chromophores: An azaborine candidate and general small size effects," *J. Phys. Chem. Lett.* **7**, 1351–1358 (2016).
- ⁷T. Polivka and V. Sundstrom, "Dark excited states of carotenoids: Consensus and controversy," *Chem. Phys. Lett.* **477**, 1–11 (2009).
- ⁸W. Barford, *Electronic and Optical Properties of Conjugated Polymers* (Oxford University Press, Oxford, 2013).
- ⁹M. B. Smith and J. Michl, "Singlet fission," *Chem. Rev.* **110**, 6891–6936 (2010).
- ¹⁰M. B. Smith and J. Michl, "Recent advances in singlet fission," *Annu. Rev. Phys. Chem.* **64**, 361–386 (2013).
- ¹¹D. Casanova, "Theoretical modeling of singlet fission," *Chem. Rev.* **118**, 7164–7207 (2018).
- ¹²K. Miyata, F. S. Conrad-Burton, F. L. Geyer, and X. Y. Zhu, "Triplet pair states in singlet fission," *Chem. Rev.* **119**, 4261–4292 (2019).
- ¹³O. P. Dimitriev, "Dynamics of excitons in conjugated molecules and organic semiconductor systems," *Chem. Rev.* **122**, 8487–8593 (2022).
- ¹⁴W. Shockley and H. J. Queisser, "Detailed balance limit of efficiency of $p-n$ junction solar cells," *J. Appl. Phys.* **32**, 510–519 (1961).
- ¹⁵T. Zeng, N. Ananth, and R. Hoffmann, "Seeking small molecules for singlet fission: A heteroatom substitution strategy," *J. Am. Chem. Soc.* **136**, 12638–12647 (2014).
- ¹⁶K. Lee and T. Gan, "Influence of substrate temperature on the optical properties of evaporated films of pentacene," *Chem. Phys. Lett.* **51**, 120–124 (1977).
- ¹⁷L. Sebastian, G. Weiser, and H. Bassler, "Charge transfer transitions in solid tetracene and pentacene studied by electroabsorption," *Chem. Phys.* **61**, 125–135 (1981).
- ¹⁸M. Rei Vilar, M. Heyman, and M. Schott, "Spectroscopy of low-energy electrons backscattered from an organic solid surface: Pentacene," *Chem. Phys. Lett.* **94**, 522–526 (1983).
- ¹⁹C. Jundt, G. Klein, B. Sipp, J. Le Moigne, M. Joucla, and A. Villaey, "Exciton dynamics in pentacene thin films studied by pump-probe spectroscopy," *Chem. Phys. Lett.* **241**, 84–88 (1995).
- ²⁰A. Troisi and G. Orlandi, "Band structure of the four pentacene polymorphs and effect on the hole mobility at low temperature," *J. Phys. Chem. B* **109**, 1849–1856 (2005).
- ²¹H. Marciniaik, M. Fiebig, M. Huth, S. Schiefer, B. Nickel, F. Selmaier, and S. Lochbrunner, "Ultrafast exciton relaxation in microcrystalline pentacene films," *Phys. Rev. Lett.* **99**, 176402 (2007).
- ²²H. Marciniaik, I. Pugliesi, B. Nickel, and S. Lochbrunner, "Ultrafast singlet and triplet dynamics in microcrystalline pentacene films," *Phys. Rev. B* **79**, 235318 (2009).
- ²³J. Johnson, A. Nozik, and J. Michl, "High triplet yield from singlet fission in a thin film of 1,3-diphenylisobenzofuran," *J. Am. Chem. Soc.* **132**, 16302–16303 (2010).
- ²⁴A. Rao, M. Wilson, J. Hodgkiss, S. Albert-Seifried, H. Bassler, and R. Friend, "Exciton fission and charge generation via triplet excitons in pentacene/C₆₀ bilayers," *J. Am. Chem. Soc.* **132**, 12698–12703 (2010).
- ²⁵C. Wang and M. Tauber, "High-yield singlet fission in a zeaxanthin aggregate observed by picosecond resonance Raman spectroscopy," *J. Am. Chem. Soc.* **132**, 13988–13991 (2010).
- ²⁶T. S. Kuhlman, J. Kongsted, K. V. Mikkelsen, K. B. Møller, and T. I. Sølling, "Interpretation of the ultrafast photoinduced processes in pentacene thin films," *J. Am. Chem. Soc.* **132**, 3431–3439 (2010).
- ²⁷P. Zimmerman, Z. Zhang, and C. Musgrave, "Singlet fission in pentacene through multi-exciton quantum states," *Nat. Chem.* **2**, 648–652 (2010).
- ²⁸J. Burdett, D. Gosztola, and C. Bardeen, "The dependence of singlet exciton relaxation on excitation density and temperature in polycrystalline tetracene thin films: Kinetic evidence for a dark intermediate state and implications for singlet fission," *J. Chem. Phys.* **135**, 214508 (2011).
- ²⁹W. Chan, M. Ligges, A. Jalaubekov, L. Kaake, L. Miaja-Avila, and X. Zhu, "Observing the multie exciton state in singlet fission and ensuing ultrafast multielectron transfer," *Science* **334**, 1541–1545 (2011).
- ³⁰M. Wilson, A. Rao, J. Clark, R. Kumar, D. Brida, G. Cerullo, and R. Friend, "Ultrafast dynamics of exciton fission in polycrystalline pentacene," *J. Am. Chem. Soc.* **133**, 11830–11833 (2011).
- ³¹P. Zimmerman, F. Bell, D. Casanova, and M. Head-Gordon, "Mechanism for singlet fission in pentacene and tetracene: From single exciton to two triplets," *J. Am. Chem. Soc.* **133**, 19944–19952 (2011).
- ³²A. Rao, M. Wilson, S. Albert-Seifried, R. Di Pietro, and R. Friend, "Photophysics of pentacene thin films: The role of exciton fission and heating effects," *Phys. Rev. B* **84**, 195411 (2011).
- ³³H. Yamagata, J. Norton, E. Hontz, Y. Olivier, D. Beljonne, J. Bredas, R. Silbey, and F. Spano, "The nature of singlet excitons in oligoacene molecular crystals," *J. Chem. Phys.* **134**, 204703 (2011).
- ³⁴W.-L. Chan, M. Ligges, and X.-Y. Zhu, "The energy barrier in singlet fission can be overcome through coherent coupling and entropic gain," *Nat. Chem.* **4**, 840–845 (2012).
- ³⁵W. Chan, J. Tritsch, and X. Zhu, "Harvesting singlet fission for solar energy conversion: One- versus two-electron transfer from the quantum mechanical superposition," *J. Am. Chem. Soc.* **134**, 18295–18302 (2012).
- ³⁶J. J. Burdett and C. J. Bardeen, "Quantum beats in crystalline tetracene delayed fluorescence due to triplet pair coherences produced by direct singlet fission," *J. Am. Chem. Soc.* **134**, 8597–8607 (2012).
- ³⁷S. T. Roberts, R. E. McAnally, J. N. Mastron, D. H. Webber, M. T. Whited, R. L. Brutney, M. E. Thompson, and S. E. Bradforth, "Efficient singlet fission discovered in a disordered acene film," *J. Am. Chem. Soc.* **134**, 6388–6400 (2012).
- ³⁸L. Ma, K. Zhang, C. Kloc, H. Sun, M. Michel-Beyerle, and G. Gurzadyan, "Singlet fission in rubrene single crystal: Direct observation by femtosecond pump-probe spectroscopy," *Phys. Chem. Chem. Phys.* **14**, 8307–8312 (2012).
- ³⁹C. Wang, M. Angeletta, C. Kuo, and M. Tauber, "Singlet fission in carotenoid aggregates: Insights from transient absorption spectroscopy," *Proc. SPIE* **8459**, 845905 (2012).
- ⁴⁰M. Wilson, A. Rao, K. Johnson, S. Gelinas, R. di Pietro, J. Clark, and R. Friend, "Temperature-independent singlet exciton fission in tetracene," *J. Am. Chem. Soc.* **135**, 16680–16688 (2013).
- ⁴¹M. Tayebjee, R. Clady, and T. Schmidt, "The exciton dynamics in tetracene thin films," *Phys. Chem. Chem. Phys.* **15**, 14797–14805 (2013).
- ⁴²J. Lee, M. Bruzek, N. Thompson, M. Sfeir, J. Anthony, and M. Baldo, "Singlet exciton fission in a hexacene derivative," *Adv. Mater.* **25**, 1445–1448 (2013).
- ⁴³C. Nelson, N. Monahan, and X. Zhu, "Exceeding the Shockley–Queisser limit in solar energy conversion," *Energy Environ. Sci.* **6**, 3508–3519 (2013).
- ⁴⁴X. Wen, P. Yu, C. Yuan, X. Ma, and J. Tang, "Singlet and triplet carrier dynamics in rubrene single crystal," *J. Phys. Chem. C* **117**, 17741–17747 (2013).
- ⁴⁵J. Mastron, S. Roberts, R. McAnally, M. Thompson, and S. Bradforth, "Aqueous colloidal acene nanoparticles: A new platform for studying singlet fission," *J. Phys. Chem. B* **117**, 15519–15526 (2013).
- ⁴⁶C. Wong, S. Penwell, B. Cotts, R. Noriega, H. Wu, and N. Ginsberg, "Revealing exciton dynamics in a small-molecule organic semiconducting film with sub-domain transient absorption microscopy," *J. Phys. Chem. C* **117**, 22111–22122 (2013).

- ⁴⁷B. Walker, A. Musser, D. Beljonne, and R. Friend, "Singlet exciton fission in solution," *Nat. Chem.* **5**, 1019–1024 (2013).
- ⁴⁸J. Lee, P. Jadhav, P. D. Reusswig, S. R. Yost, N. J. Thompson, D. N. Congreve, E. Hontz, T. Van Voorhis, and M. A. Baldo, "Singlet exciton fission photovoltaics," *Acc. Chem. Res.* **46**, 1300–1311 (2013).
- ⁴⁹P. M. Zimmerman, C. B. Musgrave, and M. Head-Gordon, "A correlated electron view of singlet fission," *Acc. Chem. Res.* **46**, 1339–1347 (2013).
- ⁵⁰S. Sharifzadeh, P. Darancet, L. Kronik, and J. Neaton, "Low-energy charge-transfer excitons in organic solids from first-principles: The case of pentacene," *J. Phys. Chem. Lett.* **4**, 2197–2201 (2013).
- ⁵¹B. Zhang, C. Zhang, R. Wang, Z. Tan, Y. Liu, W. Guo, X. Zhai, Y. Cao, X. Wang, and M. Xiao, "Nonlinear density dependence of singlet fission rate in tetracene films," *J. Phys. Chem. Lett.* **5**, 3462–3467 (2014).
- ⁵²J. Schrauben, J. Ryerson, J. Michl, and J. Johnson, "Mechanism of singlet fission in thin films of 1,3-diphenylisobenzofuran," *J. Am. Chem. Soc.* **136**, 7363–7373 (2014).
- ⁵³K. Kolata, T. Breuer, G. Witte, and S. Chatterjee, "Molecular packing determines singlet exciton fission in organic semiconductors," *ACS Nano* **8**, 7377–7383 (2014).
- ⁵⁴E. Busby, T. C. Berkelbach, B. Kumar, A. Chernikov, Y. Zhong, H. Hlaing, X.-Y. Zhu, T. F. Heinz, M. S. Hybertsen, M. Y. Sfeir, D. R. Reichman, C. Nuckolls, and O. Yaffe, "Multiphonon relaxation slows singlet fission in crystalline hexacene," *J. Am. Chem. Soc.* **136**, 10654–10660 (2014).
- ⁵⁵F. Ambrosio and A. Troisi, "Singlet fission in linear chains of molecules," *J. Chem. Phys.* **141**, 204703 (2014).
- ⁵⁶S. Yost, J. Lee, M. Wilson, T. Wu, D. McMahon, R. Parkhurst, N. Thompson, D. Congreve, A. Rao, K. Johnson, M. Sfeir, M. Bawendi, T. Swager, R. Friend, M. Baldo, and T. Van Voorhis, "A transferable model for singlet-fission kinetics," *Nat. Chem.* **6**, 492–497 (2014).
- ⁵⁷D. Casanova, "Electronic structure study of singlet fission in tetracene derivatives," *J. Chem. Theory Comput.* **10**, 324–334 (2014).
- ⁵⁸A. Musser, M. Liebel, C. Schnedermann, T. Wende, T. Kehoe, A. Rao, and P. Kukura, "Evidence for conical intersection dynamics mediating ultrafast singlet exciton fission," *Nat. Phys.* **11**, 352–357 (2015).
- ⁵⁹E. Busby, J. Xia, Q. Wu, J. Z. Low, R. Song, J. R. Miller, X.-Y. Zhu, L. M. Campos, and M. Y. Sfeir, "A design strategy for intramolecular singlet fission mediated by charge-transfer states in donor–acceptor organic materials," *Nat. Mater.* **14**, 426–433 (2015).
- ⁶⁰H. Tamura, M. Huix-Rotllant, I. Burghardt, Y. Olivier, and D. Beljonne, "First-principles quantum dynamics of singlet fission: Coherent versus thermally activated mechanisms governed by molecular π stacking," *Phys. Rev. Lett.* **115**, 107401 (2015).
- ⁶¹N. Monahan and X.-Y. Zhu, *Annu. Rev. Phys. Chem.* **66**, 601–618 (2015), edited by M. Johnson and T. Martinez.
- ⁶²K. Aryanpour, A. Shukla, and S. Mazumdar, "Theory of singlet fission in polyenes, acene crystals, and covalently linked acene dimers," *J. Phys. Chem. C* **119**, 6966–6979 (2015).
- ⁶³P. B. Coto, S. Sharifzadeh, J. B. Neaton, and M. Thoss, "Low-lying electronic excited states of pentacene oligomers: A comparative electronic structure study in the context of singlet fission," *J. Chem. Theory Comput.* **11**, 147–156 (2015).
- ⁶⁴G. B. Piland and C. J. Bardeen, "How morphology affects singlet fission in crystalline tetracene," *J. Phys. Chem. Lett.* **6**, 1841–1846 (2015).
- ⁶⁵J. Herz, T. Buckup, F. Paulus, J. U. Engelhart, U. H. Bunz, and M. Motzkus, "Unveiling singlet fission mediating states in TIPS-pentacene and its aza derivatives," *J. Phys. Chem. A* **119**, 6602–6610 (2015).
- ⁶⁶A. Bakulin, S. Morgan, J. Alster, D. Egorova, A. Chin, D. Zigmantas, and A. Rao, "Vibrational coherence reveals the role of dark multiexciton states in ultrafast singlet exciton fission," *Ultrafast Phenomena XIX: Proceedings of the 19th International Conference, Okinawa Convention Center, Okinawa, Japan, July 7–11, 2014* (Springer, Cham, 2015), pp. 226–229.
- ⁶⁷J. Zirzlmeier, R. Casillas, R. Reddy, P. B. Coto, D. Lehnher, E. T. Chernick, I. Papadopoulos, M. Thoss, R. R. Tykwinski, and D. M. Guldin, "Solution-based intramolecular singlet fission in cross-conjugated pentacene dimers," *Nanoscale* **8**, 10113–10123 (2016).
- ⁶⁸B. S. Basel, J. Zirzlmeier, C. Hetzer, B. T. Phelan, M. D. Krzyaniak, S. R. Reddy, P. B. Coto, N. E. Horwitz, R. M. Young, F. J. White, F. Hampel, T. Clark, M. Thoss, R. Tykwinski, M. R. Wasielewski, and D. M. Guldin, "Unified model for singlet fission within a non-conjugated covalent pentacene dimer," *Nat. Commun.* **8**, 15171 (2017).
- ⁶⁹F. A. Y. N. Schröder, D. H. P. Turban, A. J. Musser, N. D. M. Hine, and A. W. Chin, "Multi-dimensional tensor network simulation of open quantum dynamics in singlet fission," *arXiv.1710.01362* (2017).
- ⁷⁰Y. Fujihashi, L. Chen, A. Ishizaki, J. Wang, and Y. Zhao, "Effect of high-frequency modes on singlet fission dynamics," *J. Chem. Phys.* **146**, 044101 (2017).
- ⁷¹N. R. Monahan, D. Sun, H. Tamura, K. W. Williams, B. Xu, Y. Zhong, B. Kumar, C. Nuckolls, A. R. Harutyunyan, G. Chen *et al.*, "Dynamics of the triplet-pair state reveals the likely coexistence of coherent and incoherent singlet fission in crystalline hexacene," *Nat. Chem.* **9**, 341–346 (2017).
- ⁷²I. Breen, R. Tempelaar, L. A. Bimazima, B. Kloss, D. R. Reichman, and D. B. Turner, "Triplet separation drives singlet fission after femtosecond correlated triplet pair production in rubrene," *J. Am. Chem. Soc.* **139**, 11745–11751 (2017).
- ⁷³S. R. Reddy, P. B. Coto, and M. Thoss, "Quantum dynamical simulation of intramolecular singlet fission in covalently coupled pentacene dimers," *J. Chem. Phys.* **151**, 044307 (2019).
- ⁷⁴F. A. Y. N. Schröder, D. H. P. Turban, A. J. Musser, N. D. M. Hine, and A. W. Chin, "Tensor network simulation of multi-environmental open quantum dynamics via machine learning and entanglement renormalisation," *Nat. Commun.* **10**, 1062 (2019).
- ⁷⁵R. Casillas, M. Adam, P. B. Coto, A. R. Waterloo, J. Zirzlmeier, S. R. Reddy, F. Hampel, R. McDonald, R. R. Tykwinski, M. Thoss, and D. M. Guldin, "Intermolecular singlet fission in unsymmetrical derivatives of pentacene in solution," *Adv. Energy Mater.* **9**, 1802221 (2019).
- ⁷⁶H.-G. Duan, A. Jha, X. Li, V. Tiwari, H. Ye, P. K. Nayak, X.-L. Zhu, Z. Li, T. J. Martinez, M. Thorwart, and R. J. D. Miller, "Intermolecular vibrations mediate ultrafast singlet fission," *Sci. Adv.* **6**, eabb0052 (2020).
- ⁷⁷K. E. Smyser and J. D. Eaves, "Singlet fission for quantum information and quantum computing: The parallel JDE model," *Sci. Rep.* **10**, 18480 (2020).
- ⁷⁸J. Han, D. R. Rehn, T. Buckup, and A. Dreuw, "Evaluation of single-reference DFT-based approaches for the calculation of spectroscopic signatures of excited states involved in singlet fission," *J. Phys. Chem. A* **124**, 8446–8460 (2020).
- ⁷⁹S. Mardazad, Y. Xu, X. Yang, M. Grundner, U. Schollwöck, H. Ma, and S. Paekel, "Quantum dynamics simulation of intramolecular singlet fission in covalently linked tetracene dimer," *J. Chem. Phys.* **155**, 194101 (2021).
- ⁸⁰R. Zhao, C. P. Hettich, X. Chen, and J. Gao, "Minimal-active-space multistate density functional theory for excitation energy involving local and charge transfer states," *npj Comput. Mater.* **7**, 148 (2021).
- ⁸¹Y. Bai, W. Ni, K. Sun, L. Chen, L. Ma, Y. Zhao, G. G. Gurzadyan, and M. F. Gelin, "Plenty of room on the top: Pathways and spectroscopic signatures of singlet fission from upper singlet states," *J. Phys. Chem. Lett.* **13**, 11086–11094 (2022).
- ⁸²D. Claudio, B. Peng, K. Kowalski, and T. S. Humble, "Modeling singlet fission on a quantum computer," *J. Phys. Chem. Lett.* **14**, 5511–5516 (2023).
- ⁸³P. E. Teichen and J. D. Eaves, "A microscopic model of singlet fission," *J. Phys. Chem. B* **116**, 11473–11481 (2012).
- ⁸⁴D. Beljonne, H. Yamagata, J. Bredas, F. Spano, and Y. Olivier, "Charge-transfer excitations steer the Davydov splitting and mediate singlet exciton fission in pentacene," *Phys. Rev. Lett.* **110**, 226402 (2013).
- ⁸⁵T. C. Berkelbach, M. S. Hybertsen, and D. R. Reichman, "Microscopic theory of singlet exciton fission. I. General formulation," *J. Chem. Phys.* **138**, 114102 (2013).
- ⁸⁶T. C. Berkelbach, M. S. Hybertsen, and D. R. Reichman, "Microscopic theory of singlet exciton fission. II. Application to pentacene dimers and the role of superexchange," *J. Chem. Phys.* **138**, 114103 (2013).
- ⁸⁷S. M. Parker, T. Seideman, M. A. Ratner, and T. Shiozaki, "Model Hamiltonian analysis of singlet fission from first principles," *J. Phys. Chem. C* **118**, 12700–12705 (2014).
- ⁸⁸T. C. Berkelbach, M. S. Hybertsen, and D. R. Reichman, "Microscopic theory of singlet exciton fission. III. Crystalline pentacene," *J. Chem. Phys.* **141**, 074705 (2014).
- ⁸⁹T. Zeng, R. Hoffmann, and N. Ananth, "The low-lying electronic states of pentacene and their roles in singlet fission," *J. Am. Chem. Soc.* **136**, 5755–5764 (2014).

- ⁹⁰J. Arago and A. Troisi, "Dynamics of the excitonic coupling in organic crystals," *Phys. Rev. Lett.* **114**, 026402 (2015).
- ⁹¹C. Yang and C. Hsu, "First-principle characterization for singlet fission couplings," *J. Phys. Chem. Lett.* **6**, 1925–1929 (2015).
- ⁹²G. Tao, "Understanding electronically non-adiabatic relaxation dynamics in singlet fission," *J. Chem. Theory Comput.* **11**, 28–36 (2015).
- ⁹³H. Zang, Y. Zhao, and W. Liang, "Quantum interference in singlet fission: J- and H-aggregate behavior," *J. Phys. Chem. Lett.* **8**, 5105–5112 (2017).
- ⁹⁴X. Li, R. M. Parrish, and T. J. Martinez, "An *ab initio* exciton model for singlet fission," *J. Chem. Phys.* **153**, 184116 (2020).
- ⁹⁵X. Xie, A. Santana-Bonilla, W. Fang, C. Liu, A. Troisi, and H. Ma, "Exciton–phonon interaction model for singlet fission in prototypical molecular crystals," *J. Chem. Theory Comput.* **15**, 3721–3729 (2019).
- ⁹⁶K. Sun, Z. Huang, M. F. Gelin, L. Chen, and Y. Zhao, "Monitoring of singlet fission via two-dimensional photon-echo and transient-absorption spectroscopy: Simulations by multiple Davydov trial states," *J. Chem. Phys.* **151**, 114102 (2019).
- ⁹⁷K. Sun, Q. Xu, L. Chen, M. F. Gelin, and Y. Zhao, "Temperature effects on singlet fission dynamics mediated by a conical intersection," *J. Chem. Phys.* **153**, 194106 (2020).
- ⁹⁸K.-W. Sun and Y. Yao, "Beating maps of singlet fission: Simulation of coherent two-dimensional electronic spectroscopy by Davydov ansatz in organic molecules," *J. Chem. Phys.* **147**, 224905 (2017).
- ⁹⁹Z. Huang, Y. Fujihashi, and Y. Zhao, "Effect of off-diagonal exciton–phonon coupling on intramolecular singlet fission," *J. Phys. Chem. Lett.* **8**, 3306–3312 (2017).
- ¹⁰⁰K. Sun, X. Liu, W. Hu, M. Zhang, G. Long, and Y. Zhao, "Singlet fission dynamics and optical spectra of pentacene and its derivatives," *Phys. Chem. Chem. Phys.* **23**, 12654–12667 (2021).
- ¹⁰¹C. Schnedermann, A. M. Alvertis, T. Wende, S. Lukman, J. Feng, F. A. Y. N. Schröder, D. H. P. Turban, J. Wu, N. D. M. Hine, N. C. Greenham, A. W. Chin, A. Rao, P. Kukura, and A. J. Musser, "A molecular movie of ultrafast singlet fission," *Nat. Commun.* **10**, 4207 (2019).
- ¹⁰²I. Paci, J. Johnson, X. Chen, G. Rana, D. Popović, D. David, A. Nozik, M. Ratner, and J. Michl, "Singlet fission for dye-sensitized solar cells: Can a suitable sensitizer be found?," *J. Am. Chem. Soc.* **128**, 16546–16553 (2006).
- ¹⁰³E. C. Greyson, J. Vura-Weis, J. Michl, and M. A. Ratner, "Maximizing singlet fission in organic dimers: Theoretical investigation of triplet yield in the regime of localized excitation and fast coherent electron transfer," *J. Phys. Chem. B* **114**, 14168–14177 (2010).
- ¹⁰⁴E. Greyson, B. Stepp, X. Chen, A. Schwerin, I. Paci, M. Smith, A. Akdag, J. Johnson, A. Nozik, J. Michl, and M. Ratner, "Singlet exciton fission for solar cell applications: Energy aspects of interchromophore coupling," *J. Phys. Chem. B* **114**, 14223–14232 (2010).
- ¹⁰⁵X. Feng, A. Luzanov, and A. Krylov, "Fission of entangled spins: An electronic structure perspective," *J. Phys. Chem. Lett.* **4**, 3845–3852 (2013).
- ¹⁰⁶A. Troisi and G. Orlandi, "Dynamics of the intermolecular transfer integral in crystalline organic semiconductors," *J. Phys. Chem. A* **110**, 4065–4070 (2006).
- ¹⁰⁷W.-L. Chan, T. C. Berkelbach, M. R. Provorose, N. R. Monahan, J. R. Tritsch, M. S. Hybertsen, D. R. Reichman, J. Gao, and X.-Y. Zhu, "The quantum coherent mechanism for singlet fission: Experiment and theory," *Acc. Chem. Res.* **46**, 1321–1329 (2013).
- ¹⁰⁸M. Zarea, D. Powell, N. Renaud, M. Wasielewski, and M. Ratner, "Decoherence and quantum interference in a four-site model system: Mechanisms and turnovers," *J. Phys. Chem. B* **117**, 1010–1020 (2013).
- ¹⁰⁹G. Tao, "Bath effect in singlet fission dynamics," *J. Phys. Chem. C* **118**, 27258–27264 (2014).
- ¹¹⁰G. Tao, "Electronically nonadiabatic dynamics in singlet fission: A quasi-classical trajectory simulation," *J. Phys. Chem. C* **118**, 17299–17305 (2014).
- ¹¹¹A. V. Akimov and O. V. Prezhdo, "Nonadiabatic dynamics of charge transfer and singlet fission at the pentacene/C₆₀ interface," *J. Am. Chem. Soc.* **136**, 1599–1608 (2014).
- ¹¹²M. T. Trinh, Y. Zhong, Q. Chen, T. Schiros, S. Jockusch, M. Y. Sfeir, M. Steigerwald, C. Nuckolls, and X. Zhu, "Intra- to intermolecular singlet fission," *J. Phys. Chem. C* **119**, 1312–1319 (2015).
- ¹¹³S. Strong and J. Eaves, "Tetracene aggregation on polar and nonpolar surfaces: Implications for singlet fission," *J. Phys. Chem. Lett.* **6**, 1209–1215 (2015).
- ¹¹⁴J. Zheng, Y. Xie, S. Jiang, and Z. Lan, "Ultrafast nonadiabatic dynamics of singlet fission: Quantum dynamics with the multilayer multiconfigurational time-dependent Hartree (ML-MCTDH) method," *J. Phys. Chem. C* **120**, 1375–1389 (2016).
- ¹¹⁵F. Mirjani, N. Renaud, N. Gorczak, and F. C. Grozema, "Theoretical investigation of singlet fission in molecular dimers: The role of charge transfer states and quantum interference," *J. Phys. Chem. C* **118**, 14192–14199 (2014).
- ¹¹⁶N. Renaud and F. C. Grozema, "Intermolecular vibrational modes speed up singlet fission in perylene diimide crystals," *J. Phys. Chem. Lett.* **6**, 360–365 (2015).
- ¹¹⁷T. Shiozaki, W. Györffy, P. Celani, and H.-J. Werner, "Communication: Extended multi-state complete active space second-order perturbation theory: Energy and nuclear gradients," *J. Chem. Phys.* **135**, 081106 (2011).
- ¹¹⁸U. Schollwöck, "The density-matrix renormalization group in the age of matrix product states," *Ann. Phys.* **326**, 96–192 (2011).
- ¹¹⁹S. Paechel, T. Köhler, A. Swoboda, S. R. Manmana, U. Schollwöck, and C. Hubig, "Time-evolution methods for matrix-product states," *Ann. Phys.* **411**, 167998 (2019).
- ¹²⁰W. Domcke, D. Yarkony, and H. Köppel, *Conical Intersections: Electronic Structure, Dynamics & Spectroscopy* (World Scientific, 2004), Vol. 15.
- ¹²¹J. Prior, A. W. Chin, S. F. Huelga, and M. B. Plenio, "Efficient simulation of strong system-environment interactions," *Phys. Rev. Lett.* **105**, 050404 (2010).
- ¹²²I. V. Oseledets, "Tensor-train decomposition," *SIAM J. Sci. Comput.* **33**, 2295–2317 (2011).
- ¹²³C. Lubich, T. Rohwedder, R. Schneider, and B. Vandereycken, "Dynamical approximation by hierarchical tucker and tensor-train tensors," *SIAM J. Matrix Anal. Appl.* **34**, 470–494 (2013).
- ¹²⁴S. M. Greene and V. S. Batista, "Tensor-train split-operator Fourier transform (TT-SOFT) method: Multidimensional nonadiabatic quantum dynamics," *J. Chem. Theory Comput.* **13**, 4034–4042 (2017).
- ¹²⁵J. Ren, W. Li, T. Jiang, and Z. Shuai, "A general automatic method for optimal construction of matrix product operators using bipartite graph theory," *J. Chem. Phys.* **153**, 000153 (2020).
- ¹²⁶S. Schieber, M. Huth, A. Dobrinevski, and B. Nickel, "Determination of the crystal structure of substrate-induced pentacene polymorphs in fiber structured thin films," *J. Am. Chem. Soc.* **129**, 10316–10317 (2007).
- ¹²⁷M. Frisch, G. Trucks, H. Schlegel, G. Scuseria, M. Robb, J. Cheeseman, G. Scalmani, V. Barone, G. Petersson, H. Nakatsuji *et al.*, *Gaussian 16, Revision A. 03*, Gaussian, Inc., Wallingford CT, 2016, Vol. 3.
- ¹²⁸T. Shiozaki, "BAGEL: Brilliantly advanced general electronic-structure library," *WIREs Comput. Mol. Sci.* **8**, e1331 (2018).
- ¹²⁹Q. Shi, Y. Xu, Y. Yan, and M. Xu, "Efficient propagation of the hierarchical equations of motion using the matrix product state method," *J. Chem. Phys.* **148**, 174102 (2018).
- ¹³⁰A. W. Chin, A. Rivas, S. F. Huelga, and M. B. Plenio, "Exact mapping between system-reservoir quantum models and semi-infinite discrete chains using orthogonal polynomials," *J. Math. Phys.* **51**, 092109 (2010).
- ¹³¹I. de Vega and M.-C. Banuls, "Thermofield-based chain-mapping approach for open quantum systems," *Phys. Rev. A* **92**, 052116 (2015).
- ¹³²X. Xie, Y. Liu, Y. Yao, U. Schollwöck, C. Liu, and H. Ma, "Time-dependent density matrix renormalization group quantum dynamics for realistic chemical systems," *J. Chem. Phys.* **151**, 224101 (2019).
- ¹³³A. M. Alvertis, R. Pandya, L. A. Muscarella, N. Sawhney, M. Nguyen, B. Ehrler, A. Rao, R. H. Friend, A. W. Chin, and B. Monserrat, "Impact of exciton delocalization on exciton-vibration interactions in organic semiconductors," *Phys. Rev. B* **102**, 081122 (2020).
- ¹³⁴R. Borrelli and M. F. Gelin, "Finite temperature quantum dynamics of complex systems: Integrating thermo-field theories and tensor-train methods," *WIREs Comput. Mol. Sci.* **11**, e1539 (2021).